LA-UR-22-20021

Approved for public release; distribution is unlimited.

Title:	Final Report - High-Resolution 3D Acoustic Borehole Integrity Monitoring
Author(s):	Pantea, Cristian
Intended for:	Report
Issued:	2022-01-03

Final Report - High-Resolution 3D Acoustic Borehole Integrity Monitoring

by
Cristian Pantea

Final Report - High-Resolution 3D Acoustic Borehole Integrity Monitoring

LA-UR-21-XXXXX

Federal Agency and Organization: Office of Fossil Energy (FE); National Energy Technology Laboratory (NETL); Geologic Storage Technologies

Recipient Organization: Los Alamos National Laboratory

Project Title: High-Resolution 3D Acoustic Borehole Integrity Monitoring

Report Submitted by: Cristian Pantea
Research Scientist 4
pantea@lanl.gov
505-665-7598

Date of Report Submission: Nov 1, 2020
Reporting Period: Oct 1, 2018 to Sep 30, 2020

Project Partners:

- LANL: Cristian Pantea (PI), Dipen Sinha, Eric Davis, Vamshi Chillara, Craig Chavez, Jacob Verburg, Kai Gao, Yu Chen, Lianjie Huang
- NETL: Barbara Kutchko, Dustin Crandall
- WVU: Roger Chen
- SNL: Douglas A. Blankenship, Jiann-Cherng Su
- ORNL: Hector Santos-Villalobos, Singanallur Venkatakrishnan
- no cost-sharing partners

DOE Project Team:

DOE Project Officer – Mark Ackiewicz
Traci Rodosta
Project Monitor Mary Kylee Rice
Natalie Iannacchione

Table of Contents

EXECUTIVE SUMMARY

SubTER Topic 1. Wellbore Diagnostics and Integrity Assessment

Real-time, in-situ, high spatial resolution (sub-cm) imaging of the near-borehole environment would revolutionize wellbore diagnostics and integrity assessment by direct observation of defects. It is becoming increasingly apparent, that better understanding of the near-wellbore environment is required to meet the safety and operational needs in challenging environments such as those present in subsurface energy extraction (geothermal) and storage (CO2 sequestration) applications. Therefore, it is important to have a more robust ability to image the near-borehole and reliably detect defects.
It was proposed to further develop and improve our advanced 3D imaging system to evaluate casing defects (e.g. corrosion) and cement quality in either open- or cased-borehole with the ultimate goal to develop a commercially deployable technology. The system consists of a unique acoustic source (LANL) and advanced inversion techniques for image processing (LANL, ORNL). This system will provide comprehensive borehole integrity monitoring with improved resolution over existing techniques. As an application of this imaging system, we will characterize the effectiveness of next-generation wellbore completion technology (NETL, SNL), and will demonstrate that, unlike current technology, the proposed approach can successfully characterize foamed cements.

In FY18, the first 6 months of the project were dedicated to Phase 1: Feasibility study. Assess feasibility of the high-resolution 3D imaging technique for wellbore integrity applications, across multiple industries (geothermal, CO2 sequestration, oil & gas, nuclear repository).
In the next 6 months efforts were concentrated on Phase 2: Evaluate method on more complex wellbore environments. The main activities revolved around (1) refinement and capability enhancement of the 3D imaging system for more realistic environments, and (2) extending applicability and refining method for defects detection at the cement-formation interface.
In FY19, extensive studies were performed towards extending method beyond wellbore. More specifically, we focused on enhancing capabilities for investigation of features away from borehole. The work was divided in several distinct tasks: (1) Acoustic source improvement - develop more powerful acoustic source for deeper penetration into the formation, (2) Receivers enhancement - develop acoustic receivers with enhanced sensitivity, (3) Ruggedized tool - develop source and sensors for high temperature and high pressure operation, in corrosive environments, (4) Image processing refinement - improve image processing techniques for low S/N (signal-to-noise) ratio, (5) Technique refinement - refine the technique and enhance all detection algorithms, and (6) Enhance capabilities for foamed cements - investigate and improve detection range through foamed cements.
The FY20 efforts were geared towards developing an engineering prototype that approaches the standards required for CO_2 sequestration and geothermal industry, with FY21 concentrating on ORNL and SNL efforts to wrap up work on their respective tasks, with carry-over funding.

PROJECT OBJECTIVES

The *main objective* of this project is to develop a *high-resolution 3D imaging system* for improved wellbore diagnostics and integrity assessment, with the ultimate goal to develop a commercially deployable technology.

Comprehensive solutions to wellbore integrity monitoring and improved near wellbore fracture detection are needed in multiple energy sectors (Geothermal, CO_2 Storage, Oil & Gas, Nuclear Waste Disposal). There are several issues than can affect the integrity of a wellbore: (i) Casing-related: pitting, metal loss, thickness variation, corrosion, fractures, pipe deformation, damage on the inner wall of the casing, damage on the outer surface of the casing, casing trajectory issues, formation integrity/formation movement, over-pressure behind casing, microannuli, etc., and (ii) Cement-related: cement channeling, cement bond to pipe, cement bond to formation, cement location, strength of cement bond, formation integrity/formation movement, cement degradation, etc. Wellbore integrity monitoring and characterization of the near wellbore environment are in need of novel technologies for better, faster and safer characterization methods. Some of the goals of these methods are: (1) improved resolution, (2) extended characterization range, and (3) in-situ/real-time monitoring. We are planning to work in parallel to address all these three requirements, such that we can provide a complete solution for wellbore diagnostics and integrity assessment.

Currently, there is a technology gap between conventional sonic tools (penetrating less than a foot from the borehole with good vertical resolution) and long range sonic imaging tools, such as Schlumberger's Borehole Acoustic Reflection Survey (BARS) technique (tens of feet from the borehole with lower vertical resolution and limited azimuthal resolution, about 0.3 m). Conventional ultrasonic tools, like Schlumberger's Ultrasonic Borehole Imager (UBI), have better resolution, operate at a frequency of 250/500 kHz, and collect information only from the borehole wall. Formation changes can be detected only if borehole surface effects are present (changes in rugosity or borehole diameter). Tools similar to these discussed above are available from other service companies, including Haliburton, Archer, etc.

PROJECT APPROACH

Our proposed high-resolution imaging system takes advantages of a unique acoustic source (highly collimated, high power, broad-band: 10-150 kHz), Acoustic Collimated Beam (ACCObeam) and high-resolution imaging techniques for comprehensive borehole integrity monitoring.

ACCObeam is a unique Bessel beam acoustic source (patent pending) that generates a collimated beam with narrower frequency bandwidth and very limited diffraction (no beam spread during propagation) and self-healing properties. That is, the beam may be partially obstructed at one point, but will re-form at a point further down the beam axis.

This new acoustic imaging system can create a new technological opportunity of developing a complete borehole measurement system to extract important information for cement and reservoir evaluation. A very simplistic schematic of the hardware is shown in Figure 1. Our approach provides deeper penetration than a conventional sonic probe while providing azimuthal resolution comparable/similar to a high-frequency ultrasonic tool (3-5 millimeters). In general, the attenuation in the formation is proportional to frequency squared ($\alpha \sim f^2$). Basically, the lower the frequency, the lower the attenuation, resulting in deeper penetration into the formation. However, conventional transducers able to generate low frequency produce an acoustic

beam that has considerable beam spread, resulting in poor lateral resolution.

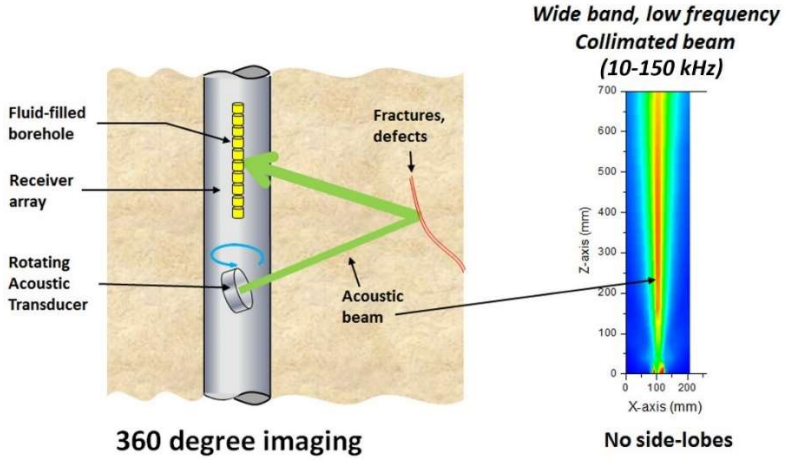

Figure 1. Schematic representation of the 3D imaging system (left), and experimental data, in water, for the collimated beam showing very low beam spread.

Figure 2 below is an illustration of the two main accomplishments: (1) *extend the investigation range* beyond the wellbore casing to the cement and further into the formation to a distance of about 3 meters, and (2) *improve the resolution* of 3D images around the borehole. The ability to characterize defect structure into the formation is an enormous advantage as it can allow analysis of the quality of the cement-formation bond that was difficult in the past, and can also determine whether drilling-induced damage exists in the adjacent formation that is not possible to detect with past technology.

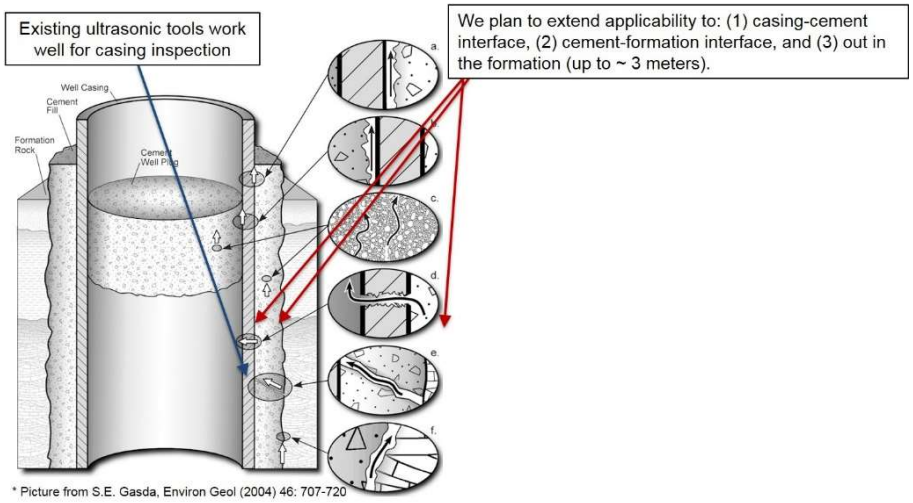

Figure 2. A schematic of potential wellbore failure modes and the investigation range of our technique vs existing ultrasonic tools.

A comparison between the present approach and existing technologies is summarized in Table 1, in terms of frequency used, expected range, and resolution.

Table 1. Comparison of existing techniques and the present approach.

Method	Frequency (kHz)	Range (m)	Resolution (mm)
Sonic probe	0.3-8	15	~ 300
Present approach	10-150	~ 3	~ 5
Ultrasonic probe	>250	casing	4-5

A key part of the technology is the acquisition of ***high-resolution images*** of the wellbore casing, cement, and geological formations behind the cement. LANL has developed a suite of unique, high-resolution seismic migration imaging and acoustic- and elastic-waveform inversion methods for subsurface imaging and reservoir characterization, including a least-squares reverse-time migration method using efficient, implicit wavefield separation to improve image resolution [1], and a least-squares reverse-time migration-guided full-waveform inversion method to greatly enhance the convergence rate and robustness of full-waveform inversion [2]. These methods have not been applied to the wellbore problem before.

Additionally, the applicability of our tool to ***foamed cements*** was investigated. The use of foamed cements has been increasing in recent years, especially for deep-water applications, being the system of choice for hazard mitigation in the Gulf of Mexico. However, limited information on foamed cement behavior at conditions specific to wellbores exists at present and conventional methods have difficulty detecting foamed cement due to low impedance contrast. A combination of LANL's acoustic characterization techniques (e.g., frequency mixing, resonance spectroscopy) for the determination of the quality of these cements and possible induced defects with computed tomography (CT) conducted on laboratory-scale wellbore systems [4-6] will lead to a better understanding of how the foamed cements behave in realistic environments.

ACCOMPLISHMENTS & MILESTONE UPDATE

Project Status Summary:
The project tasks and completion date and status of the project are summarized in Table *2*, below.
Additionally, the milestones corresponding to different tasks are summarized for clarity and easy reference in Table 3.

Table 2. Project tasks and completion date/status.

Task	Title	Planned Completion Date	Completion Date or % completion
Phase 1 - Feasibility study			
1	Investigation of existing technology	03/31/2018	100%
2	Define metrics	03/31/2018	100%
3	Industry partners/technology maturation plan	03/31/2018	100%
Phase 2 - Evaluate method on more complex wellbore environments			
1	Channeling outside casing	09/30/2018	100%
2	Hardware/software refinement	09/30/2018	100%
3	Speed-up measurement & analysis	09/30/2018	100%
4	Method testing on more complex wellbore environments	09/30/2018	100%
5	Foamed cements manufacturing	09/30/2018	100%
6	CT of foamed cements	09/30/2018	100%
7	Acoustics metrics of foamed cements	09/30/2018	100%
8	Tests on simulated wellbores with foamed cements	09/30/2018	52%
Phase 3 - Extend method beyond wellbore			
1	Acoustic source improvement	03/31/2019	100%
2	Receivers enhancement	03/31/2019	100%
3	Ruggedized tool	09/30/2019	100%
4	Image processing enhancement	09/30/2019	100%
5	Technique refinement	09/30/2019	100%
6	Enhance capabilities for foamed cements	09/30/2019	100%
Phase 4 – Technology development and verification			
1	Prototype development	09/30/2020	100%
2	Prototype verification at lab scale and in field	09/30/2020	95%
3	Hardware/software enhancement and refinement	09/30/2020	100%

Table 3. Project tasks and milestones.

Task	Year 1				Year 2				Year 3			
	Q1	Q2	Q3	Q4	Q1	Q2	Q3	Q4	Q1	Q2	Q3	Q4
Phase 1 - Feasibility study												
Task 1 – Investigation of existing technology		M2										
Task 2 – Define metrics	M1											
Task 3 – Industry partners/technology maturation plan												
	GoNoGo1											
Phase 2 - Evaluate method on more complex wellbore environments												
Task 1 - Channeling outside casing			M3									
Task 2 - Hardware/software refinement												
Task 3 - Speed-up measurement & analysis												
Task 4 - Method testing on more complex wellbore environments				M4								
Task 5 - Foamed cements manufacturing												
Task 6 - CT of foamed cements												
Task 7 - Acoustics metrics of foamed cements												
Task 8 - Tests on simulated wellbores with foamed cements				M4								
			GoNoGo2									
Phase 3 - Extend method beyond wellbore												
Task 1 - Acoustic source improvement					M5							
Task 2 - Receivers enhancement												
Task 3 - Ruggedized tool							M7					
Task 4 - Image processing refinement						M6						
Task 5 - Technique refinement								M8				
Task 6 - Enhance capabilities for foamed cements												
							GoNoGo3					
							GoNoGo4					
Phase 4 - Technology Development and Verification												
Task 1 - Prototype development									M9			
Task 2 - Prototype verification at lab scale and in field											M11	
Task 3 - Hardware/software enhancement and refinement										M10		

**Obs: purple arrows show interdependencies between different tasks, while yellow arrows show milestones that lead to main Go/No-Go decision points.*

Definition of milestones and Go/No-Go points:

[Milestone 1 – M1]

[Description: Identify key performance metrics that will be used to judge success in subsequent phases of the project]

[Responsible individual or partner: LANL, NETL, ORNL, SNL]

[Planned completion date: end of Y1/Q1]

[Deliverable and milestone verification method: key performance metrics identified – resolution, penetration depth, resistance to adverse conditions]

[Milestone 2 – M2]
[Description: Identify baseline performance of existing technologies, validated through elicitation of industry input, case studies, and/or literature review]
[Responsible individual or partner: LANL, NETL, ORNL, SNL]
[Planned completion date: end of Y1/Q2]
[Deliverable and milestone verification method: Identified and assessed existing commercial technology. Go to *Go/No-Go1*]

[Milestone 3 – M3]
[Description: Investigate the ability to detect fluid and/or fluid flow through channels outside the casing]
[Responsible individual or partner: LANL]
[Planned completion date: end of Y1/Q3]
[Deliverable and milestone verification method: generated experimental data from channeling outside casing, and qualitatively determined if fluid detection is possible]

[Milestone 4 – M4]
[Description: Carry out extensive testing both in the lab and/or at other appropriate test facilities on both neat cements and foamed cements]
[Responsible individual or partner: LANL, SNL]
[Planned completion date: end of Y1/Q4]
[Deliverable and milestone verification method: performed successful tests on wellbores with foamed cements, with similar resolution as for neat cements. Go to *Go/No-Go2*]

[Milestone 5 – M5]
[Description: Develop more powerful acoustic source for deeper penetration into the formation]
[Responsible individual or partner: LANL]
[Planned completion date: end of Y2/Q1]
[Deliverable and milestone verification method: identified materials and made steps toward improving the power of the acoustic source by a factor of at least 1.5]

[Milestone 6 – M6]
[Description: Improve image processing techniques for low S/N (signal-to-noise) ratio]
[Responsible individual or partner: LANL, ORNL]
[Planned completion date: end of Y2/Q2]
[Deliverable and milestone verification method: made positive steps toward improving S/N ratio]

[Milestone 7 – M7]
[Description: Develop source and sensors for high temperature and high pressure operation, in corrosive environments]

[Responsible individual or partner: LANL]
[Planned completion date: end of Y2/Q3]
[Deliverable and milestone verification method: tool can survive to temperatures of 250°C and high pressures (~ 45 kpsi). Go to *Go/No-Go3*]

[Milestone 8 – M8]
[Description: Refine the technique and enhance all detection algorithms]
[Responsible individual or partner: LANL, NETL, SNL]
[Planned completion date: end of Y2/Q4]
[Deliverable and milestone verification method: performed successful tests on wellbores with resolution of ~ 5mm, and penetration depth of ~ 3m. Go to *Go/No-Go4*]

[Milestone 9 – M9]
[Description: Initiate development/identify materials for an engineering prototype that can withstand adverse conditions of corrosiveness, high temperature and high pressure]
[Responsible individual or partner: LANL, SNL]
[Planned completion date: end of Y3/Q1]
[Deliverable and milestone verification method: identified materials for a prototype, and initiated the development of the prototype]

[Milestone 10 – M10]
[Description: Develop robust operation & analysis software, for near real-time 3D imaging by speeding up the measurement and analysis process]
[Responsible individual or partner: LANL, ORNL]
[Planned completion date: end of Y3/Q2]
[Deliverable and milestone verification method: enhanced and refined hardware/software such that the analysis time is reduced considerably, possible to near real-time]

[Milestone 11 – M11]
[Description: Carry out testing both in the lab and at other appropriate facilities]
[Responsible individual or partner: LANL, NETL, SNL]
[Planned completion date: end of Y3/Q3]
[Deliverable and milestone verification method: performed experiments for prototype verification in the lab and initiated experiments in the field]

[Milestone 12 – M12]
[Description: Discuss with third party vendors for technology transfer and commercialization]
[Responsible individual or partner: LANL, NETL, ORNL, SNL]
[Planned completion date: end of Y3/Q4]
[Deliverable and milestone verification method: performed commercialization study, and identified at least one potential third party vendor]

ANNUAL GO/NO-GO

[Phase 1 SMART milestone – *Go/No-Go1*]
[Description: Tabulate commercial 3D imaging techniques for borehole integrity]
[Responsible individual or partner: LANL, NETL, ORNL, SNL]
[Planned completion date: end of second quarter, first year]
[Deliverable and milestone verification method: there are no commercial technologies for high-resolution 3D imaging technology with similar depth of penetration (~3 meters) and resolution (< 5 mm)]

[Phase 2 SMART milestone – *Go/NoGo2*]
[Description: Detect defects at the cement-formation interface, with high resolution (5 mm, or better)]
[Responsible individual or partner: LANL, NETL, ORNL, SNL]
[Planned completion date: end of year 1]
[Deliverable and milestone verification method: defects detection at the cement-formation interface with a resolution of at least 5 mm]

[Phase 3 SMART milestone 1 – *Go/No-Go3*]
[Description: Tool survival in adverse conditions of corrosiveness, high temperature and high pressure (brines specific to geothermal wells, at temperatures of at least 250°C, and high pressures of up to 45 kpsi)]
[Responsible individual or partner: LANL, NETL, ORNL, SNL]
[Planned completion date: end of year 2]
[Deliverable and milestone verification method: imaging system can survive in adverse conditions of temperature, pressure and corrosiveness]

[Phase 3 SMART milestone 2 – *Go/No-Go4*]
[Description: Imaging capabilities out in the formation, up to 3 meters.]
[Responsible individual or partner: LANL, NETL, ORNL, SNL]
[Planned completion date: end of year 2]
[Deliverable and milestone verification method: defects/features (up to ~ 3m) can be resolved in the received signal]

FINAL SUCCESS METRICS

(1) Prototype in field functionality similar to the one observed in tests in the laboratory.
(2) Identified third party vendors interested in developing a commercial tool based on the technology generated from this project.

Phase 1. Feasibility study

Assess feasibility of the high-resolution 3D imaging technique for wellbore integrity applications, across multiple industries (geothermal, CO_2 sequestration, oil & gas, nuclear repository).

Task 1. Investigation of existing technology

1. **Planned Activities**:
   Baseline performance of existing technologies, validated through elicitation of industry input, case studies, and/or literature review.
2. **Actual Accomplishments**:
   Performed a comprehensive literature/existing technology study for wellbore integrity monitoring tools.

   Literature study:

   Wellbore integrity is crucial for geothermal energy production. It is necessary to monitor wellbore integrity throughout the life cycle of production/injection wells. The existing techniques for wellbore integrity monitoring include optical, electrical and acoustic imaging.

   Optical imaging uses photographic camera for visual inspection and recording of downhole completion conditions [Prensky, 1999]. It is capable of directly obtaining a high-resolution color image of the wellbore wall for fracture identification or casing inspection. The direct-imaging technology has only limited use because of the operational requirement of a transparent borehole fluid or in air holes, which are often impractical. The other drawback of optical imaging is that the technique can detect only fractures on the inner surface.

   Acoustic imaging makes use of acoustic reflectivity to detect the changes of surface roughness and fractures in the wellbore wall. Acoustic waves travel through the drilling fluid and undergo partial reflections on the borehole wall. Reflected pulses are received by a transducer. The amplitudes and travel times of the reflected pulses are influenced by several factors, such as fractures, vugs, breakouts on the borehole walls, and acoustic impedance between the fluid and the borehole walls [Zemanek et al., 1970; Massiot et al., 2015]. The wellbore televiewer can provide a 360° image in an open or cased hole. The principle limitation of current state-of-the-art of this technique is that it uses only acoustic reflections, and can detect only the inner surface of the wellbore walls.

   Electric imaging identifies fractures by contrasts in conductivity between the fracture and the adjacent borehole wall. The images are produced by placing pads with arrays of electrodes maintained at a constant electrical potential against the borehole wall, and measuring the current drop as the electrodes travel along the borehole wall. Data from multiple electrodes are combined to produce electrical conductivity images [Davatzes and Hickman, 2005]. Electric imaging tools have proved superior to the acoustic imaging in the identification of some structural features and rock properties in depth. However, acoustic imaging can reveals a higher resolution on the wellbore surface [Davatzes and Hickman, 2005].

   There are several tolls on the market, represented by three main service companies, Schlumberger, Baker Hughes, and Halliburton. Additionally, we identified a couple more tools by Archer, and Advance Logic Technology. All the tools we were able to identify on the market are summarized in APPENDIX A. A more streamlined table is presented in APPENDIX B **– Comparison Matrix**, in a

comparison table. Only three main competitors are presented, with a detailed comparison of different parameters of interest, e.g. frequency, collimation resolution.

Task 2. Define metrics

1. **Planned Activities**:
   Identify key performance metrics that will be used to judge success in subsequent phases of the project.
2. **Actual Accomplishments**:
   Identified key performance metrics, defined previously in the proposal:
   - Resolution of 5 mm, or better
   - Penetration depth of 2-3 meters
   - Resistance to adverse conditions specific to CO_2 sequestration reservoirs and geothermal wells: high temperature (up to 250°C), high pressure (up to 45 kpsi), and corrosive environment (use of materials and sealants resistant to corrosion).

   Final success metrics: prototype in field functionality similar to the one observed in tests in the laboratory.

Task 3. Industry partners/technology maturation plan

1. **Planned Activities**:
   Identify industry partners and use cases for the tools to be further developed in subsequent phases, and provide a technology maturation plan.
2. **Actual Accomplishments**:
   Identified Chevron as potential future partner for further developing the proposed technique. Obtained Support Letter from Chevron, on two different occasions: once when the proposal was submitted, and when we submitted an R&D100 application.
   Technology maturation plan is reflected in the work proposed in the third year:
   - Develop an engineering prototype. The prototype has to meet the standards required for CO_2 sequestration and geothermal industry, in terms of resistance to corrosion, high temperature and high pressure.
   - Develop robust operation & analysis software, for near real-time 3D imaging by speeding up the measurement and analysis process.

Phase 2. Evaluate method on more complex wellbore environments

Refinement and capability enhancement of the 3D imaging system for more realistic environments (casing-foamed cement-rock) and experimental validation. Extend range of investigation to cement-formation interface.

Task 1. Channeling outside casing

1. **Planned Activities**:
   Investigate the ability to detect fluid and/or fluid flow through channels outside the casing.
2. **Actual Accomplishments**:

Investigated the ability to detect either (i) a water-filed pipe, outside the casing, and (ii) density differences in the cement layer, away from the casing.

(i) Water-filled pipe

A 6 inch carbon steel pipe was embedded in a barrel filed with cement, with an external diameter of 18 inches, see Figure 3. While several features of interest were built in the cement layer, we are only interested here in the water-filled pipe on the right side of the figure, about 1 inch away from the steel pipe. The dimensions of features are as follows: cement outer diameter 460 mm, steel pipe inner diameter 148 mm, steel pipe thickness 10 mm, groove depth 50 mm, and plastic pipe location 25 mm. Several different frequencies were used, but we are showing only the results for an excitation frequency of about 112 kHz, see Figure 4. The region labeled "Water-filled pipe" shows very distinct features as compared with the overall signal.

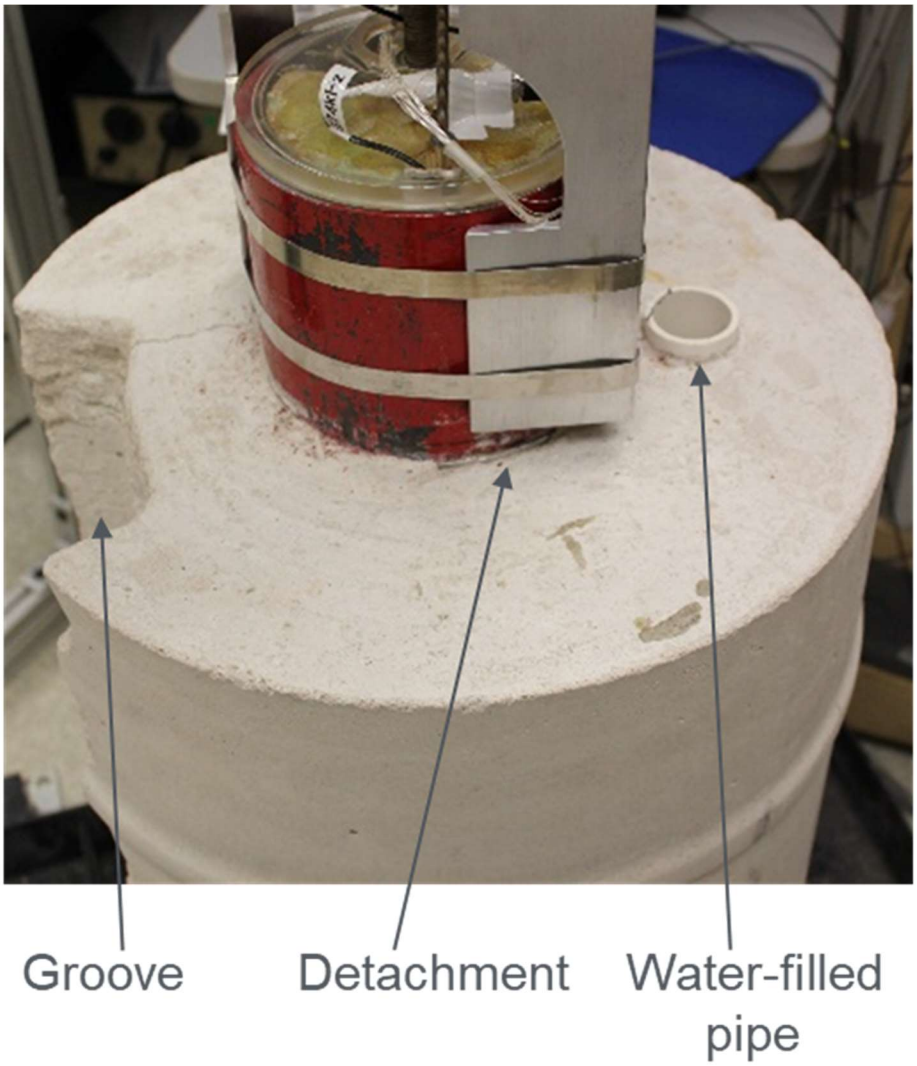

Figure 3. Simulated borehole system, in a cased borehole configuration.

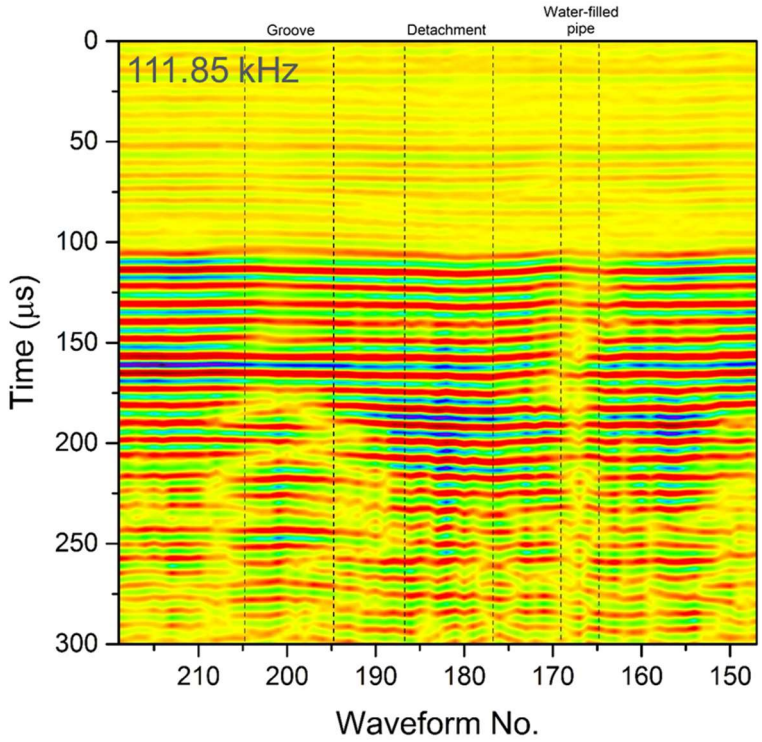

Figure 4. "Common-receiver representation" of the data collected in the cement barrel shown in Figure 3.

(ii) Density differences

Density differences were obtained from the multi-scale acoustic full-waveform inversion algorithm for velocity model, developed by the LANL software team. Data were collected using fixed azimuth, and vertical translation of source and receivers. An example is shown below, for two different excitation frequencies, Figure 5.

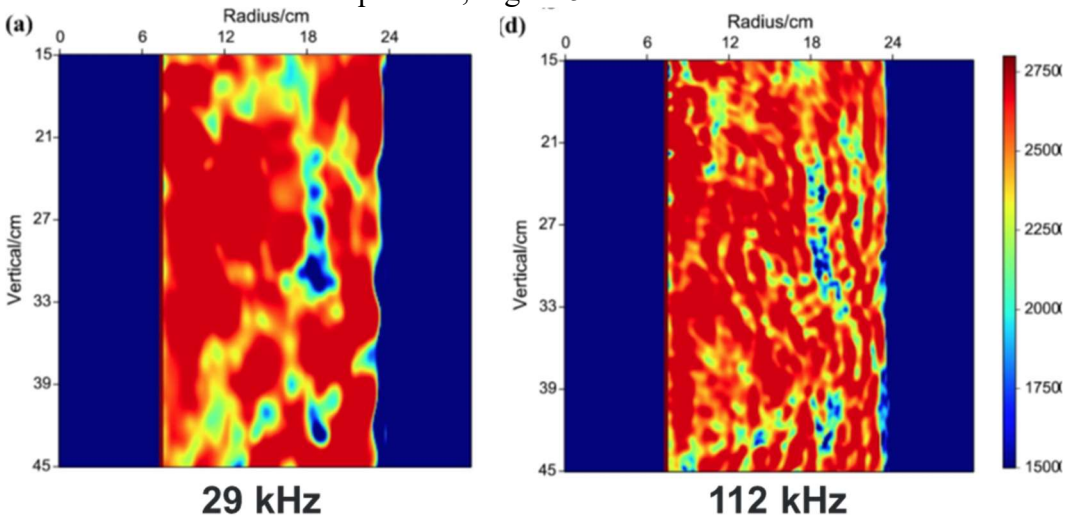

Figure 5. Densities differences in one vertical section of the cement barrel.

Task 2. Hardware/software refinement

1. **Planned Activities**:
   Refine the technique and enhance all detection algorithms
2. **Actual Accomplishments**:
   Detailed concrete heterogeneities, including a low-velocity zone, are obtained using the recently developed full-waveform inversion and least-squares reverse-time migration methods. Full-waveform inversion fits synthetic ultrasonic waveforms with recorded waveforms to build a high-resolution velocity model. Least-squares reverse-time migration produces a high-resolution structural image showing material discontinuities.

Task 3. Speed-up measurement & analysis

1. **Planned Activities**:
   Develop robust operation & analysis software, for near real-time 3D imaging by speeding up the measurement and analysis process.
2. **Actual Accomplishments**:
   Developed robust operation software, speeding up data collections to a factor of at least 10 times. Also developed improved acoustic source, significantly more powerful than its predecessor. The previous acoustic source of low-frequency collimated sound was based on acoustic nonlinear mixing, which suffers from a significant power loss, with an efficiency of 1%, at best. The present source is based on radial modes of vibration of a transducer, and does not suffer significant loos due to mixing efficiencies.

Task 4. Method testing on more complex wellbore environments

1. **Planned Activities**:
   Carry out extensive testing both in the lab and/or at other appropriate test facilities.
2. **Actual Accomplishments**:
   Performed extensive tests on two different wellbore environments: concrete barrel, and Sierra White granite.
   (i) Concrete barrel
   The concrete barrel is illustrated in *Figure 6*, with a rotational stage also capable of vertical translation. Several waveforms were collected at three different center frequencies of 29, 42, and 58 kHz for imaging concrete heterogeneities, which are resonant frequencies of the transmitter. The borehole casing is Plexiglas with a thickness of 3 mm. The inside diameter of the Plexiglas casing is 146 mm. During data acquisition, the 3D imaging prototype translates vertically along the borehole with a step size of 10 mm in a range from 10 mm to 240 mm away from the borehole bottom, acquiring data for 24 source positions. *Figure 7* shows the results of the the spatial distribution of the velocity, obtained by applying the multi-scale Full-Waveform Inversion algorithm to the deconvolved ultrasonic data.

Figure 6. Instrumented wellbore environment consisting of a Plexiglas pipe embedded in a concrete barrel.

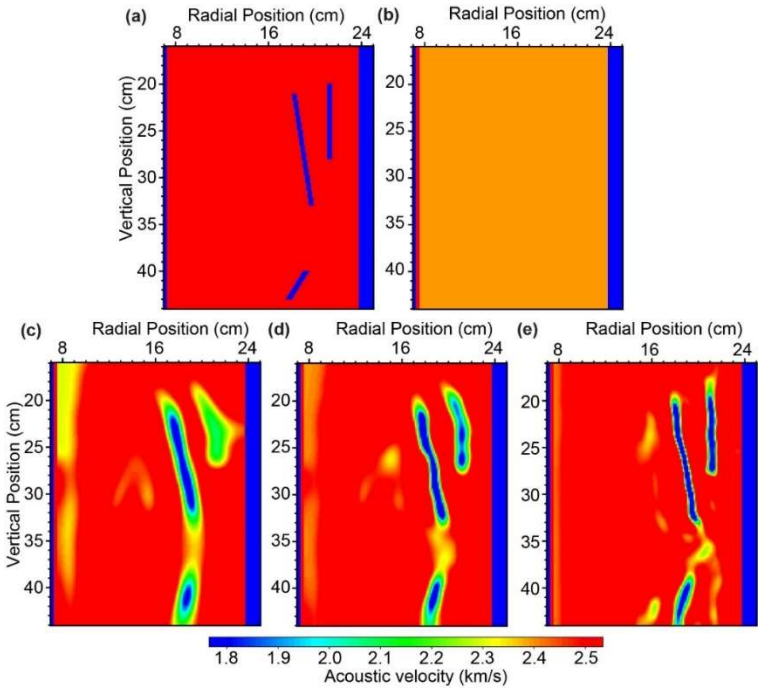

Figure 7. (a) Velocity model based on experimental data; (b) Initial velocity model used for full-waveform inversion; (c-e) Results of full-waveform inversion obtained using the center frequencies of 29 kHz (c), 42 kHz (d), and 58 kHz (e).

(ii) Sierra White granite

Four Sierra White granite blocks, with dimensions of 2 ft x 2 ft x 4 ft (width x length x height) were used. A 4 inch borehole was machined and cemented in place in the center of the granite blocks. An image of the tool as lowered in the wellbore is shown in Figure 8, while examples of the waveform collected are shown in Figure 9.

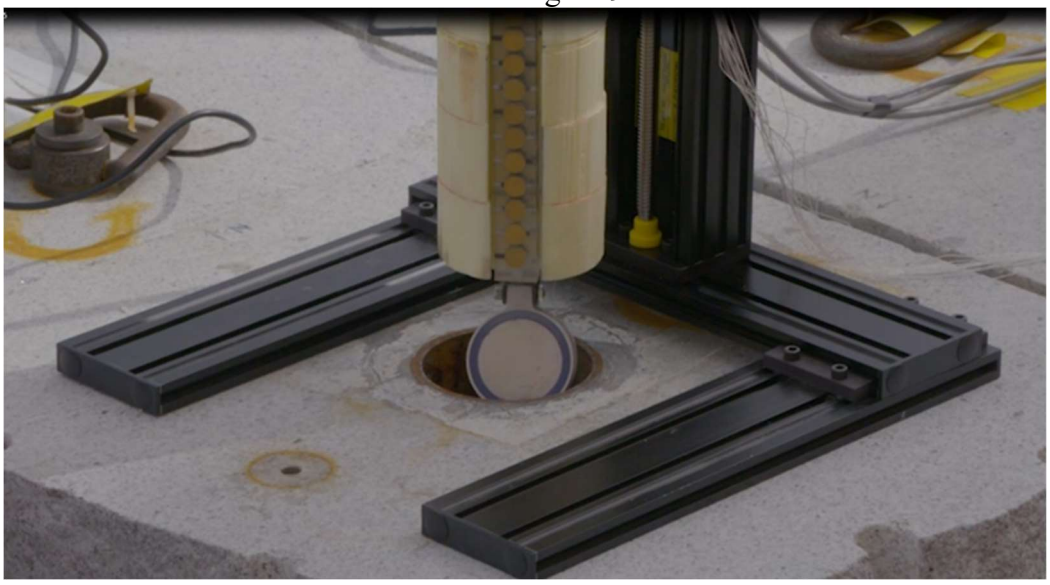

Figure 8. Lowering the imaging system in a 4" wellbore

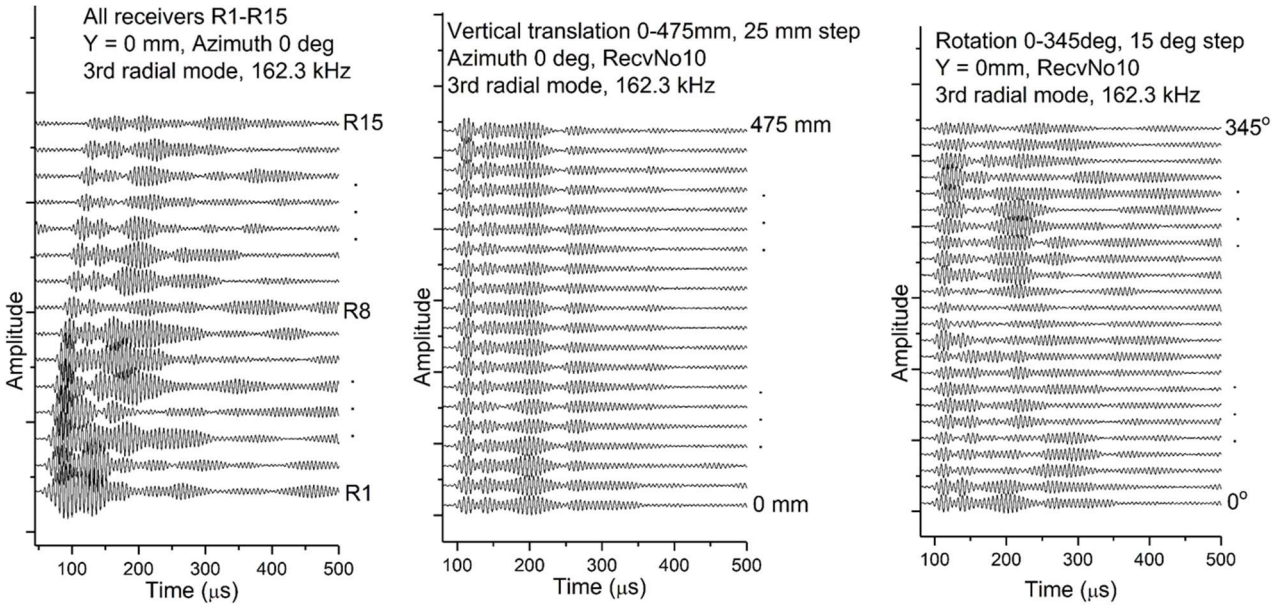

Figure 9. Example scans on granite blocks 360 deg rotation, and 475 mm vertical span 15 deg and 25 mm step size.

Task 5. Foamed cements manufacturing

1. **Planned Activities**:
   Generate neat and foamed cements at a variety of pressures and foam qualities.
2. **Actual Accomplishments**:
   An analysis of foamed cement using computed tomography scanning was conducted to examine structural differences in the bubble size distribution of foamed cements generated using two different techniques. As described in Dalton et al (2018), cements were generated using the American Petroleum Institutes recommended practice 10B-4 (API RP 10B-4) at atmospheric conditions and under elevated pressures using a novel closed loop system (de Rozières & Ferrière, 1991). Cements generated with the API RP-10B-4 tended to have larger and more spherical bubbles than those created at pressure. This suggests that when field equipment is used to mix and place foamed cements in subsurface wellbores the compressive strength and flow resistance should be superior to the behavior observed in analysis of foamed cement using the API RP 10B-4.

Dalton, L.E., Brown, S., Moore, J., Crandall, D., and Gill, M. 2018 **Laboratory Foamed Cement Curing Evolution using CT Scanning**, SPE Drilling and Completion, SPE-191843-PA. https://doi.org/10.2118/194007-PA
de Rozières, J. and Ferrière, R. 1991. **Foamed Cement Characterization under Downhole Conditions and Its Impact on Job Design**, *SPE Prod Eng* **6** (3): 297-304. SPE-19935-PA. https://doi.org/10.2118/19935-PA

Task 6. CT of foamed cements

1. **Planned Activities**:
   Characterization of foamed cements with CT (computerized tomography).
2. **Actual Accomplishments**:

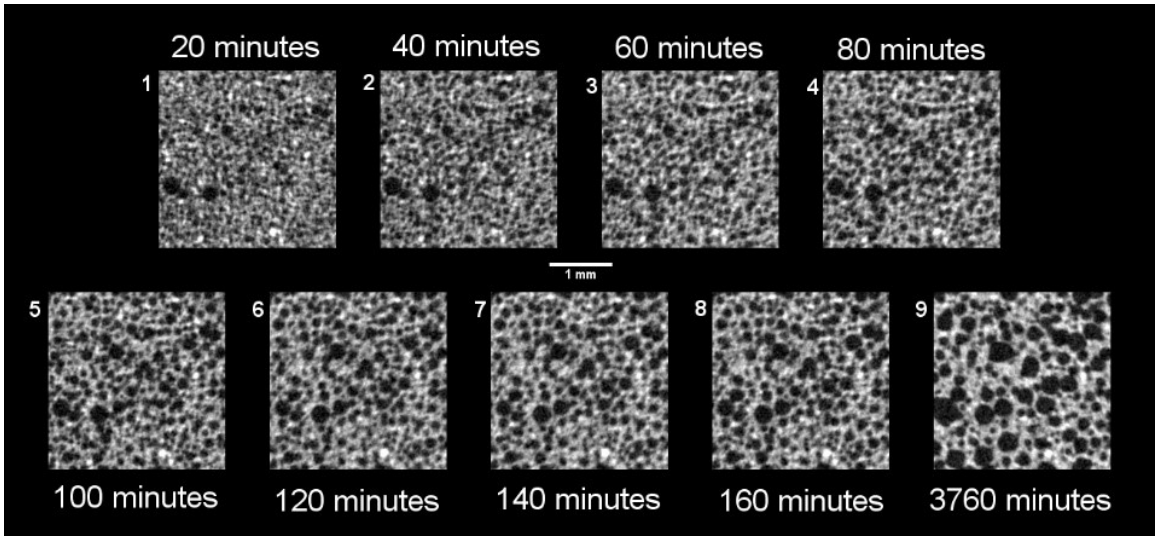

Figure 10. Time evolution of 60% gas foamed cement sample generated under pressure analyzed with computed tomography

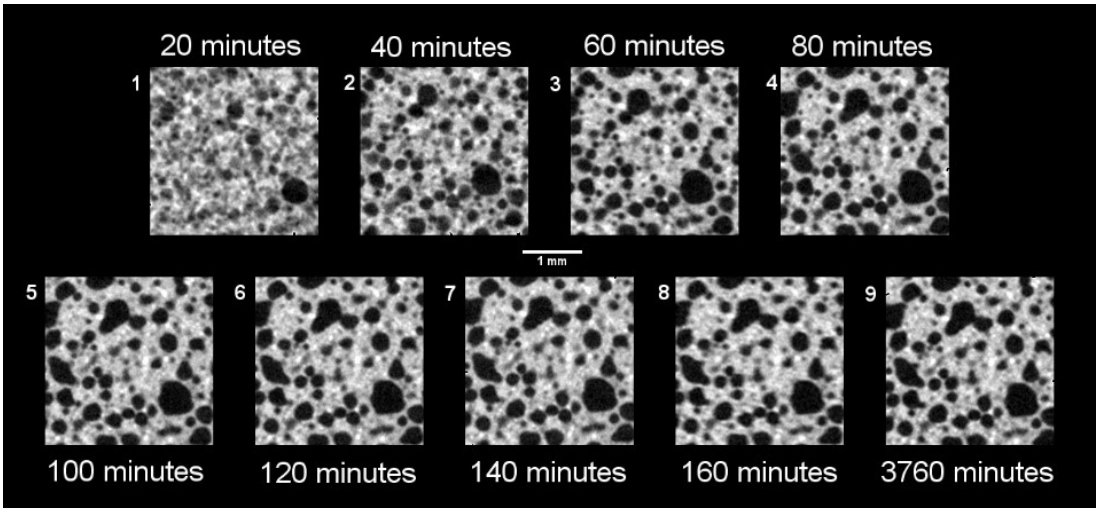

Figure 11. Time evolution of 40% gas foamed cement sample generated using the API RP 10B-4 with computed tomography

Task 7. Acoustics metrics of foamed cements

1. **Planned Activities**:
   Characterization of foamed cements with Acoustics.
2. **Actual Accomplishments**:
   A material model has been developed to compute the degree of hydration of Class H cement using the chemical composition from the Mill Test Report shown in Table 1. The percentages of the four major compounds of cement (C3S, C2S, C3A, C4AF) can be estimated based on Bogue's equations.

Table 4. Chemical composition of class H cement.

Components	CaO	SiO_2	Al_2O_3	Fe_2O_3	MgO	SO_3	Blaine (m^2/kg)	C_3S	C_2S	C_3A	C_4AF
%	64.7	22.3	2.6	4.3	2.3	2.9	310	61.7	17.3	0	12.7

The ultimate heat of hydration for the Class H cement calculated based on the formula by Lerch and Bogue can be estimated to be about 481.14 J per gram of cement.

$$H_{ultimate} = 500 \cdot p_{C_3S} + 260 \cdot p_{C_2S} + 866 \cdot p_{C_3A} + 420 \cdot p_{C_4AF} + 624 \cdot p_{SO_3} + 1186 \cdot p_{FreeCaO} + 850 \cdot p_{MgO}$$

A more detailed discussion is presented in Appendix C.

Task 8. Tests on simulated wellbores with foamed cements

1. **Planned Activities**:
   Acoustic characterization of foam cements in simulated borehole to determine the applicability of the technique for in-situ foamed cement characterization, such as cement physical property determination

and imaging of voids and cracks. Investigate enhancement of the measurement capability by incorporating nonlinear acoustics measurements.

2. **Actual Accomplishments**:
Figure 12 shows the isothermal heat measurements of foamed cement at the reference temperature of 23 °C. The isothermal calorimetry and the plastic specimen bottle that was used in the heat of hydration measurement is shown in the pictures below. The volume of each bottle was about 24.6 ml. The mix proportions that are shown in the table were calculated based on the volume of each bottle with the assumption of a water-cement ratio = 0.38 with the amount of 0.0151 ml of FAW-20 surfactant for each gram of cement. The top figure represents the heat of hydration produced by each foam quality (10%, 20%, 30% air content percentage) versus time; the heat energy reduction is proportional to the reduction of cement's mass densities in the bottle, and the bottom figure shows the amount of normalized heat by the mass of cement (joule per gram of the cement). It can be seen from this figure that foamed cement paste with different foam quality produced the same amount of heat per gram of the cement. However, the addition of the surfactant, FAW-20, delayed and reduced the early-age heat production of the foam cement. Isothermal calorimetry was also used to measure the heat of hydration of neat cement and foamed cement at higher temperatures of 33 and 43 °C as shown in Figure 13.

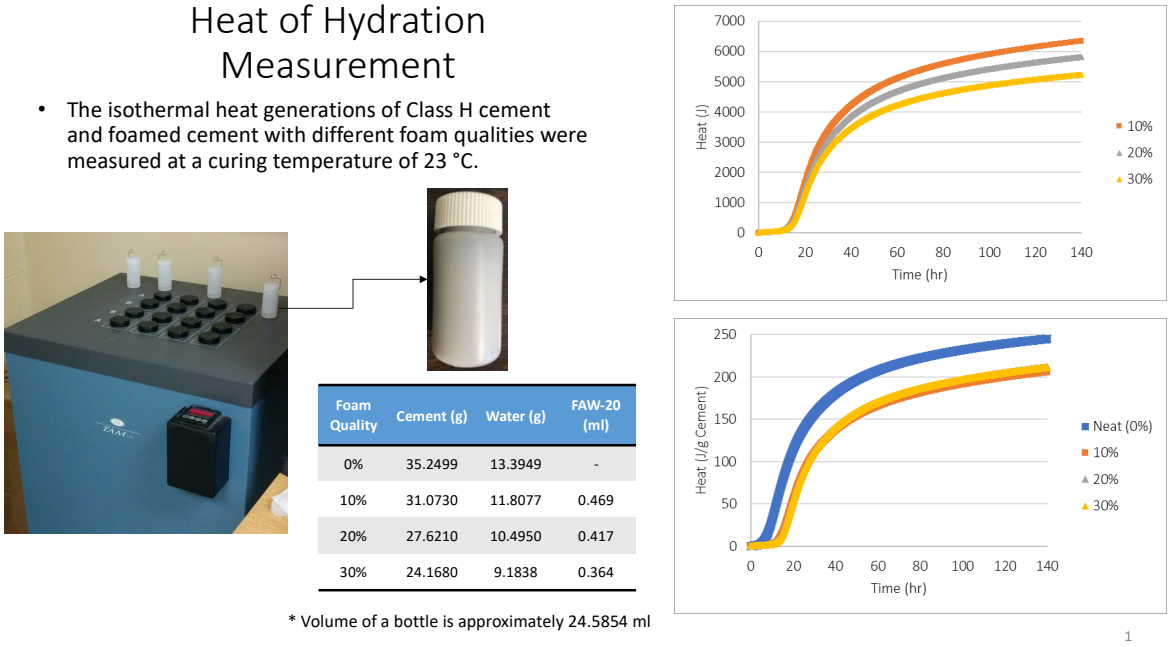

Figure 12. Heat of hydration.

Figure 13 shows the results of isothermal testing at three different curing temperatures and the calculated activation energy. Following the equation by Pang et al. (2013), two material parameters of activation energy and activation volume are needed to describe maturity at different temperature and applied pressure. The two figures in the slide represent the results of three sets of isothermal testing at different curing temperatures of 23, 33, and 43 °C. The foam cement with different qualities (10%, 20%, 30%) were found to have very

similar heat of hydration behaviors, and an average measurement is shown in the bottom figure, which was used to calculate the activation energy of foam cement. All three sets of isothermal data are fitted with an exponential function. The apparent activation energy was found using the slope of the best fit line of the natural logarithm of the slope versus the reciprocal curing temperature in Kelvin times the negative of natural gas constant. The measured activation energies were used to calculate the equivalent age of the cement paste and the foamed cement. To consider the effects of pressure on the maturity of cement paste, the activation volume will need to be experimentally measured.

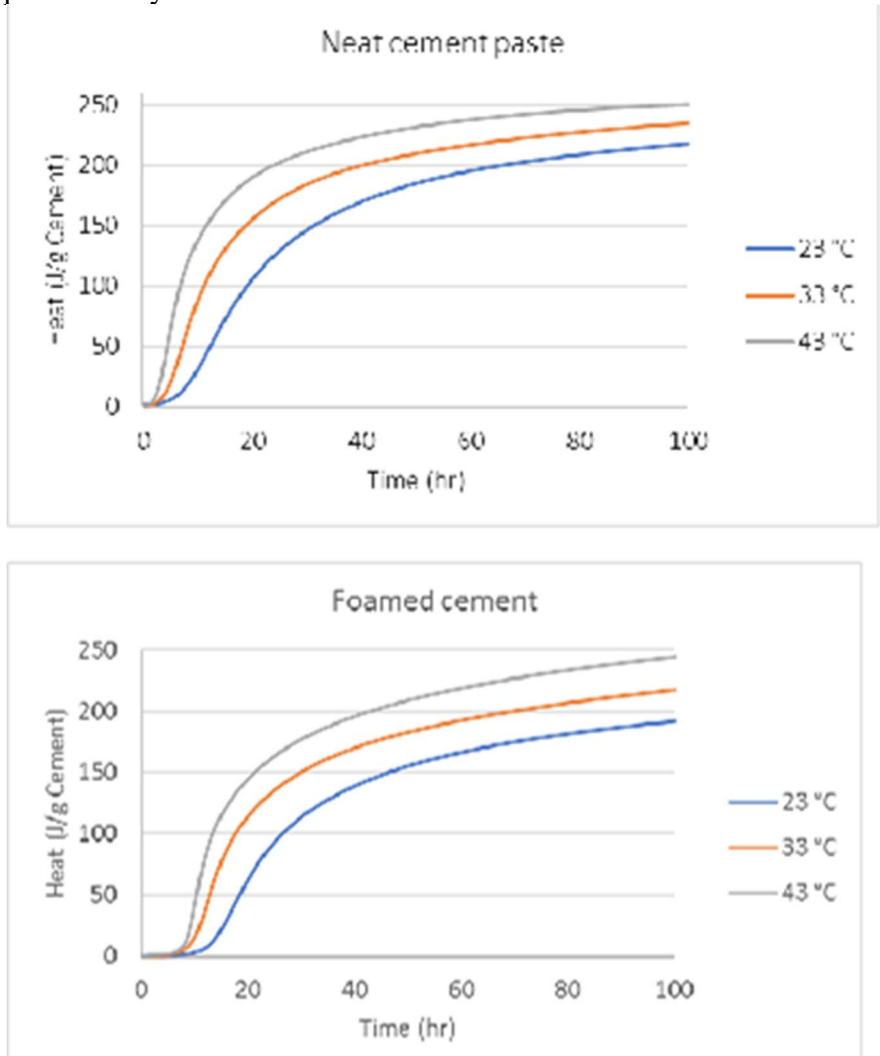

Figure 13. Isothermal heat measurements at three curing temperatures.

Figure 14 shows the test results compared with the analytical results from the material model we developed following Maekawa, et al. (2009). The material model computes the degree of hydration of Class H cement using the chemical composition of the cement. The chemical properties of Lafarge Class H cement (Joppa Plant) which were used in the calculations are based on Mill test report and are shown in the table. The material model utilizes reference heat rate and activation energy for each

cement chemical compound in the calculation. The heat generation of each compound are calculated to obtain the total heat of hydration of the cement mix. The top figure is a comparison between the measured heat and the analysis of the Class H cement. The measured heat generations from the experiments and the analytical calculations match reasonably well. The three figures at the bottom show the test results from Pang et al. (2013). By using their reported chemical minerals of Class G, Class H-P, and Class A cement (shown in the table), our material model can predict the heat generation curves. Results show that the measured heat generations from the experiments and the analytical calculations match reasonably well for different types of oil well cement. The heat of hydration is then used to calculate the degree of hydration of the binder. The calculated degree of hydration is used to calculate the mechanical properties that will be presented in next step.

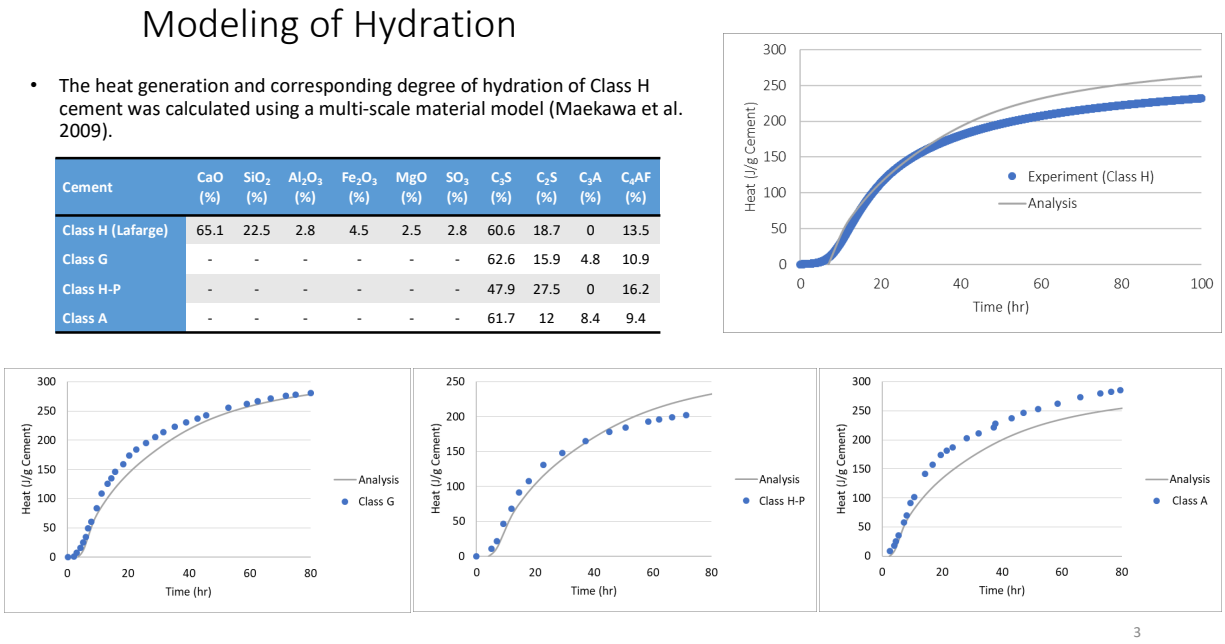

Figure 14. Hydration modeling.

Figure 15 shows the calculation of Young's modulus using the material model. The effective medium theory is the basis for the calculation of Young's modulus which assumes the cement paste is a porous medium consisting of hydration products (C-S-H gel), pores, pore water, and anhydrous cement. The early-age Young's modulus of the neat (0% foam quality) Class H cement was measured using the ultrasonic pulse velocity (UPV) method. The predicted Young's modulus of the neat Class H cement compared with the UPV test results at different equivalent age is shown. Also, the effect of having various water-cement ratios (w/c) ranging from 0.37 to 0.40 on Young's modulus of the neat Class H cement is shown. The results show that the increase of the water-cement ratio reduces the modulus of elasticity. The nonlinear relationship between the w/c ratio (from 0.35 to 0.45) and the Young's modulus of the neat Class H cement at the age of 28 days is plotted. The relationship can be fitted using a second-order polynomial function.

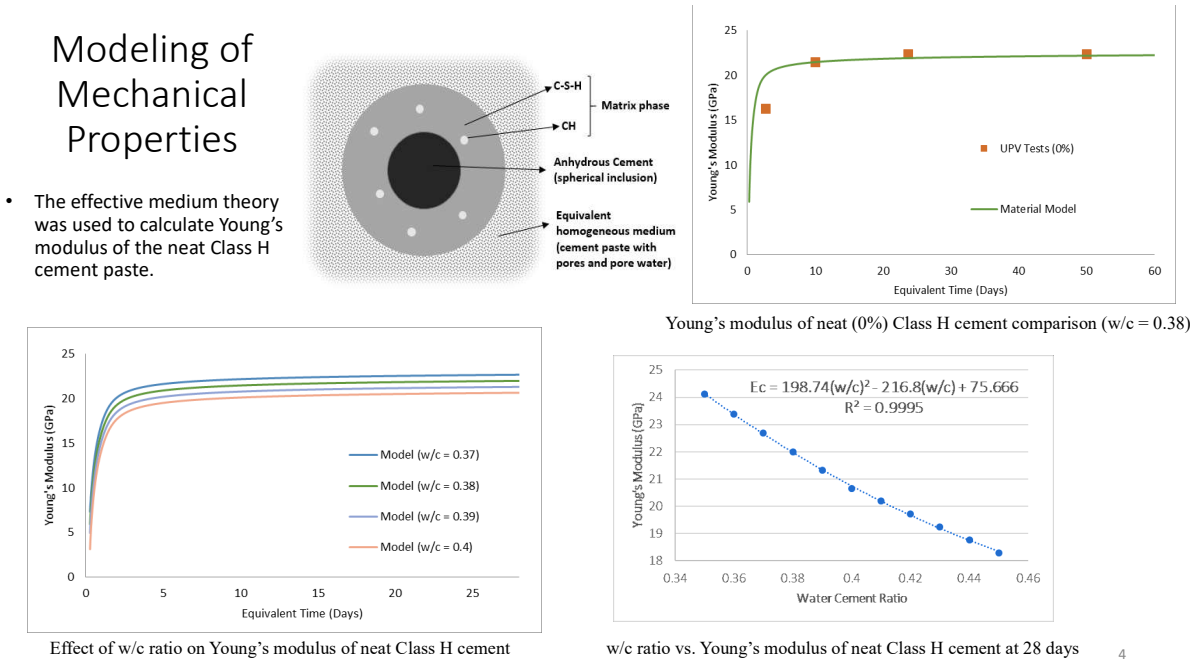

Figure 15. Mechanical properties modeling.

In slide no.5, the calculation of the Young's modulus for the foamed cement with different foam quality was developed. The Young's modulus can be predicted based on the chemical composition of the cement and the chemical admixture used in the mix. The theories based on poromechanics and composite material were used to calculate the mechanical properties of the foamed cement paste. The analysis considers that the hydrating Portland cement has the following components: Calcium silica hydrate (C-S-H) gel, calcium hydroxide (CH), anhydrous cement, capillary pores, and pore water. In addition, spherical air inclusions were added to calculate the mechanical properties of the foamed cement with different foam qualities. (The drawings shown on top of the slide from left to right indicating the three levels of the model: Level 1: cement particle level, showing hydration products (C-S-H, CH and Anhydrous cement); Level 2: cement paste level, showing numerous cement particles surrounded by pores and pore water; Level 3: foamed cement level, showing cement paste plus spherical air inclusions.)

Experimental results measured using ultrasonic tests of 40-mm (diameter) by 120-mm (length) cylinders of the neat cement and the foamed cement with different foam qualities (air void contents at approximately 10%, 20%, 30%) were shown in the figure for comparison with the prediction from our analysis. The foamed cement specimens were produced at NETL Pittsburgh Lab. The specimens were first cured inside their molds for a period of 3-days at 50 °C. After 3- days, the specimens were removed from their molds and cured for an additional 4-days at 50 °C. They were then cured for the remainder of the 28-days at 40 °C. All the cylinders were produced with the water-cement ratio of 0.38 using Class H Lafarge cement. In the calculation, the air percentages based on the average

measured mass densities of the specimens were used which is shown in the table. A good agreement was found between the analysis and the ultrasonic measurements. Results shown in the figure indicate that our material model is able to predict the development of Young's modulus of the neat cement (0% foam quality) as well as the foamed cement with different foamed qualities (15.27%, 24.82% and 33.15%) at different equivalent ages.

The graph on the bottom left shows the comparison of experimental data and the analysis at the age of 7 days (equivalent age ~ 25 days). The results show that the Young's modulus reduced with increased foam qualities. At 7-days age, the Young's modulus of a foamed cement with 20% foam quality (~11GPa) is only about 50% of the Young's modulus of the neat cement (~22GPa). During next phase, the Young's modulus and the Poisson's ratio of wellbore foamed cement at different depths will be predicted using the developed material model; the temperature and pressure at different depths will be considered using the concept of activation energy and activation volume.

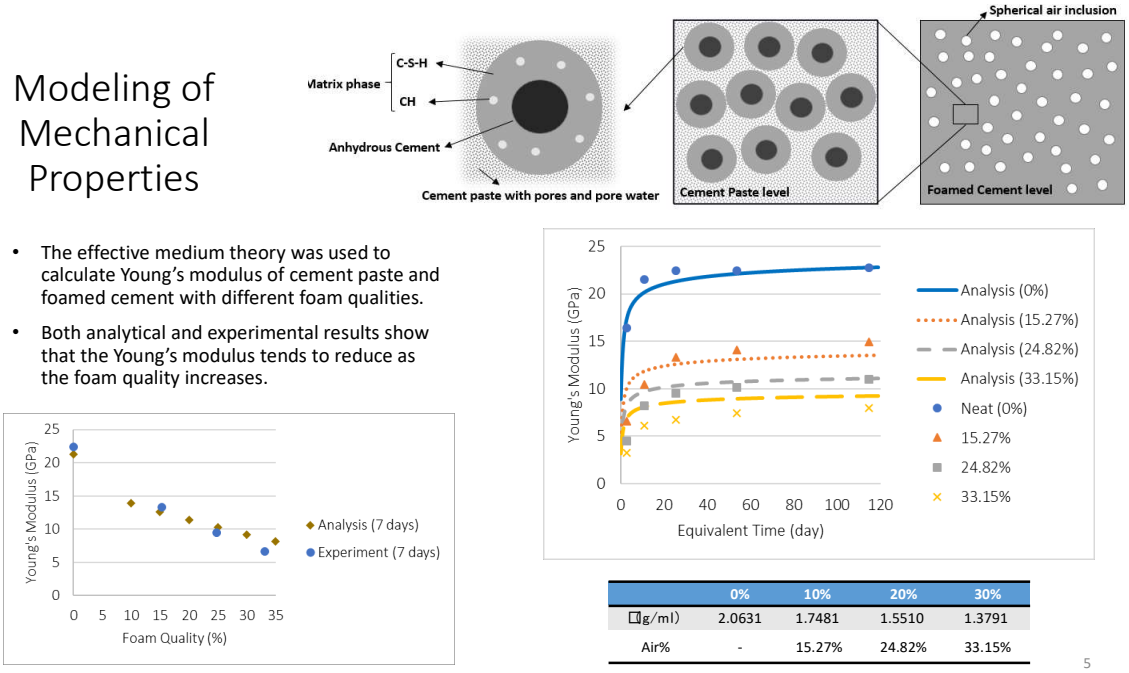

Figure 16. Mechanical properties modeling and aging.

Phase 3. Extend method beyond wellbore

Enhance capabilities for investigation of features away from borehole (up to ~ 3 m).

Task 1. Acoustic source improvement

1. **Planned Activities**:
   Develop more powerful acoustic source for deeper penetration into the formation.

2. **Actual Accomplishments**:
Increased efficiency of the acoustic source by ~2 orders of magnitude. New source is based on clamped radial modes, see below.

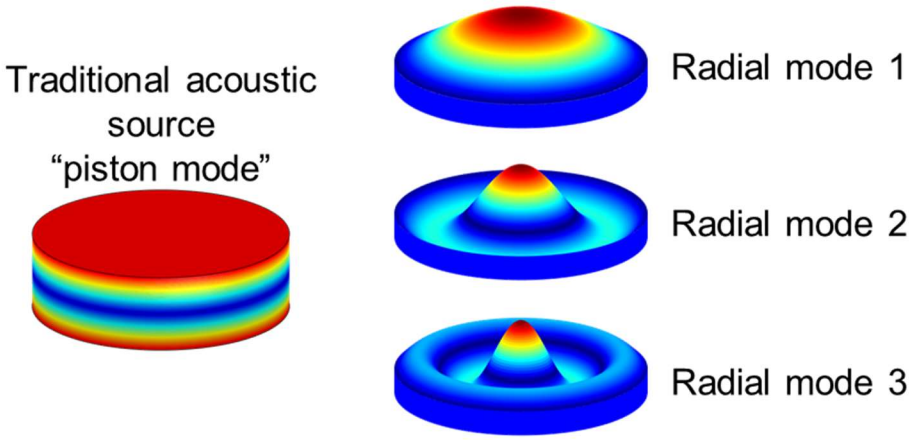

Figure 17. Illustration of 'traditional' vs radial mode of vibration of a piezoelectric transducer.

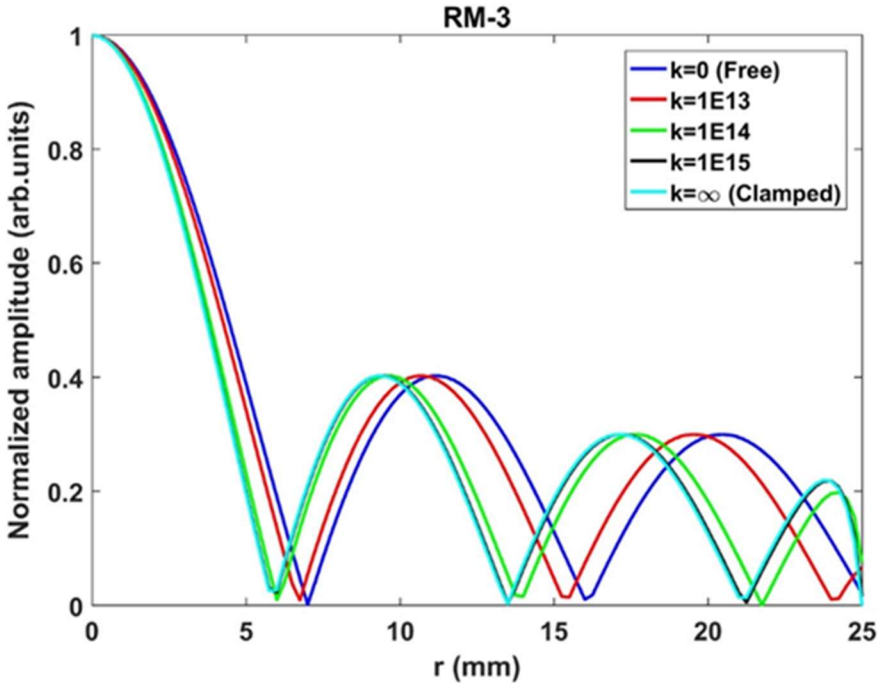

Figure 18. Normalized out-of-plane displacement on the surface of the disc for RM-3 for different lateral stiffness k (N/m3)

Finite element modeling was performed to determine the expected beam profile from different radial modes. An example is shown in Figure 19, while comparison of experimental data for traditional vs collimated low frequency acoustic source is shown in Figure 20.

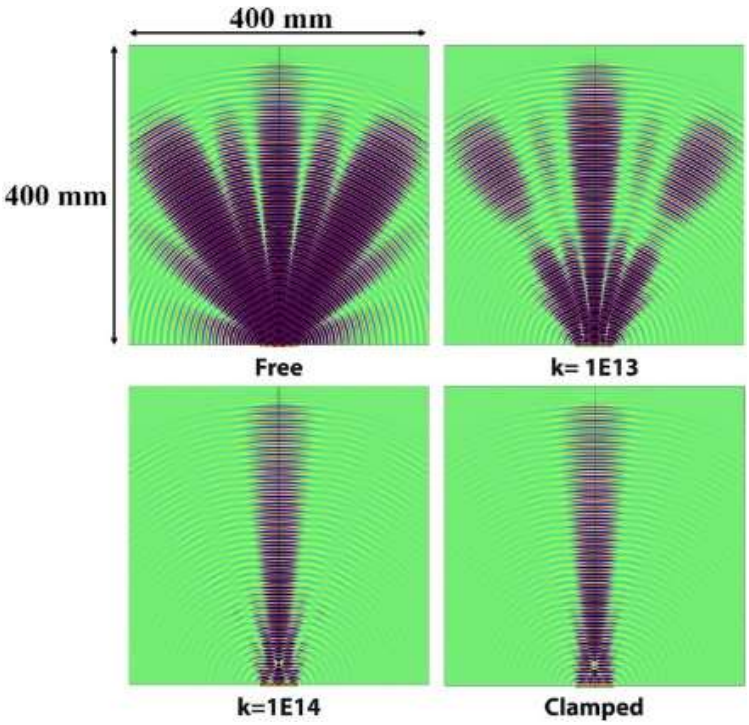

Figure 19. Theoretical model of beam profile for the third radial mode of a piezoelectric transducer.

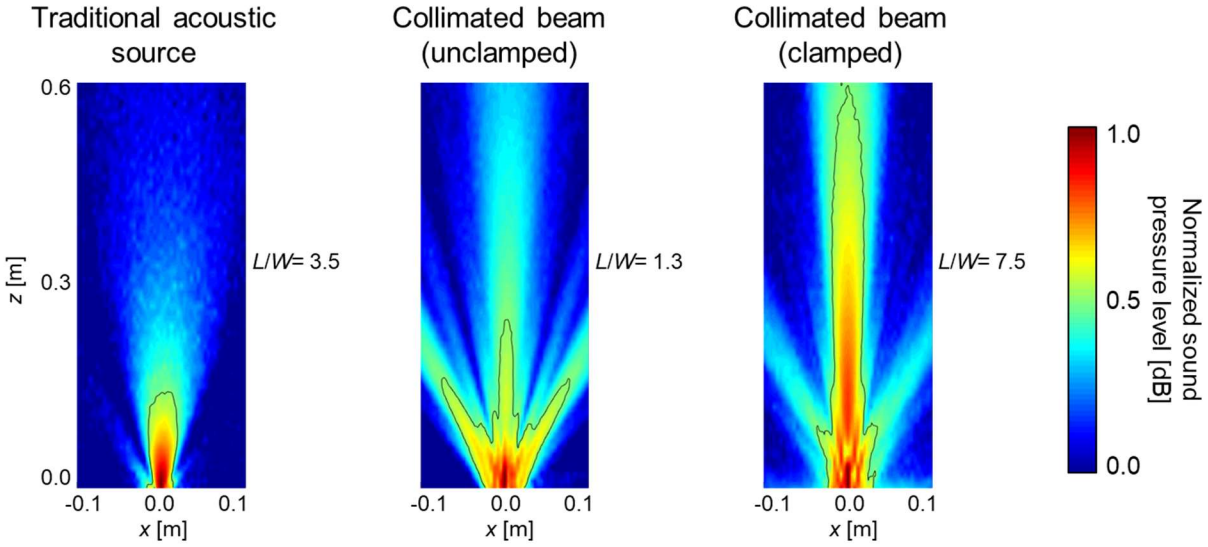

Figure 20. Experimental beam profiles.

It can be observed that a collimated beam provides (i) reduction in beam width, which leads to higher image resolution, and more control over directivity, and (ii) increased beam length, leading to longer detection/communication range.

Task 2. Receivers enhancement

1. **Planned Activities**:
   Develop acoustic receivers with enhanced sensitivity.
2. **Actual Accomplishments**:
   Enhanced receivers' sensitivity, by extending their bandwidth and using backing materials with appropriate elastic properties (IP sensitive).

Task 3. Ruggedized tool

1. **Planned Activities**:
   Develop source and sensors for high temperature and high pressure operation, in corrosive environments.
2. **Actual Accomplishments**:
   Ruggedized tool for harsh conditions (high temperature, high pressure, corrosiveness, etc.), by using materials with appropriate properties (IP sensitive).

Task 4. Image processing refinement

1. **Planned Activities**:
   Improve image processing techniques for low S/N (signal-to-noise) ratio.
2. **Actual Accomplishments**:
   LANL made significant progress toward improved image processing, resulting in accurate representation of realistic borehole. Some examples are shown below.

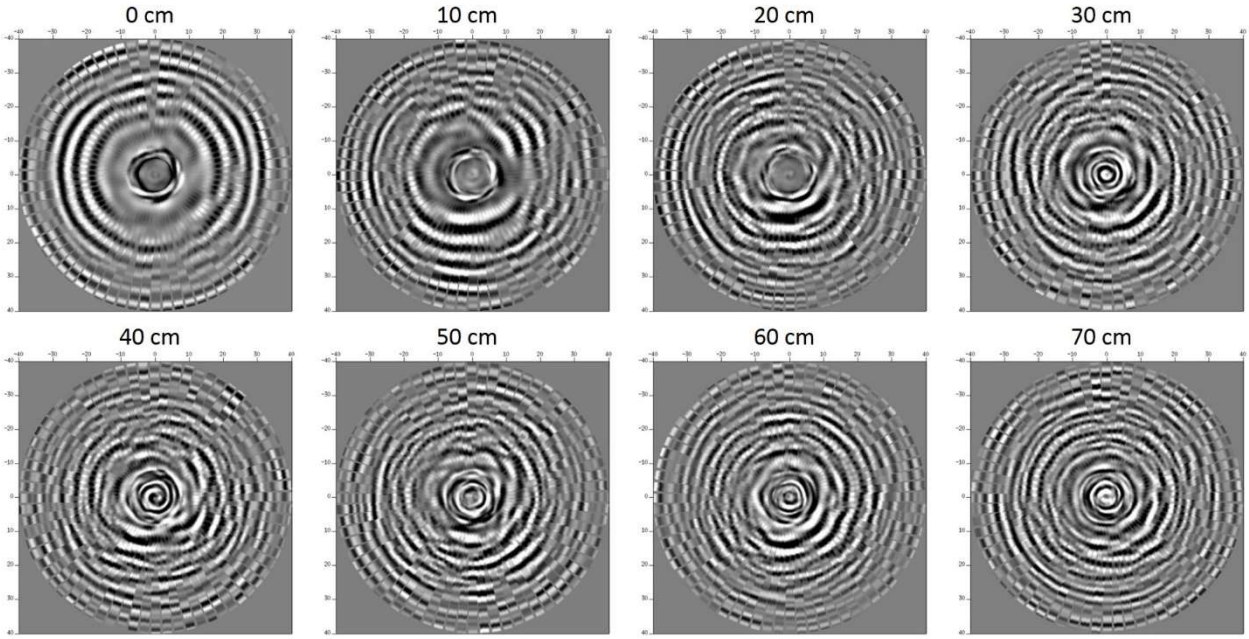

Figure 21. Horizontal slices in a steel pipe embedded in granite.

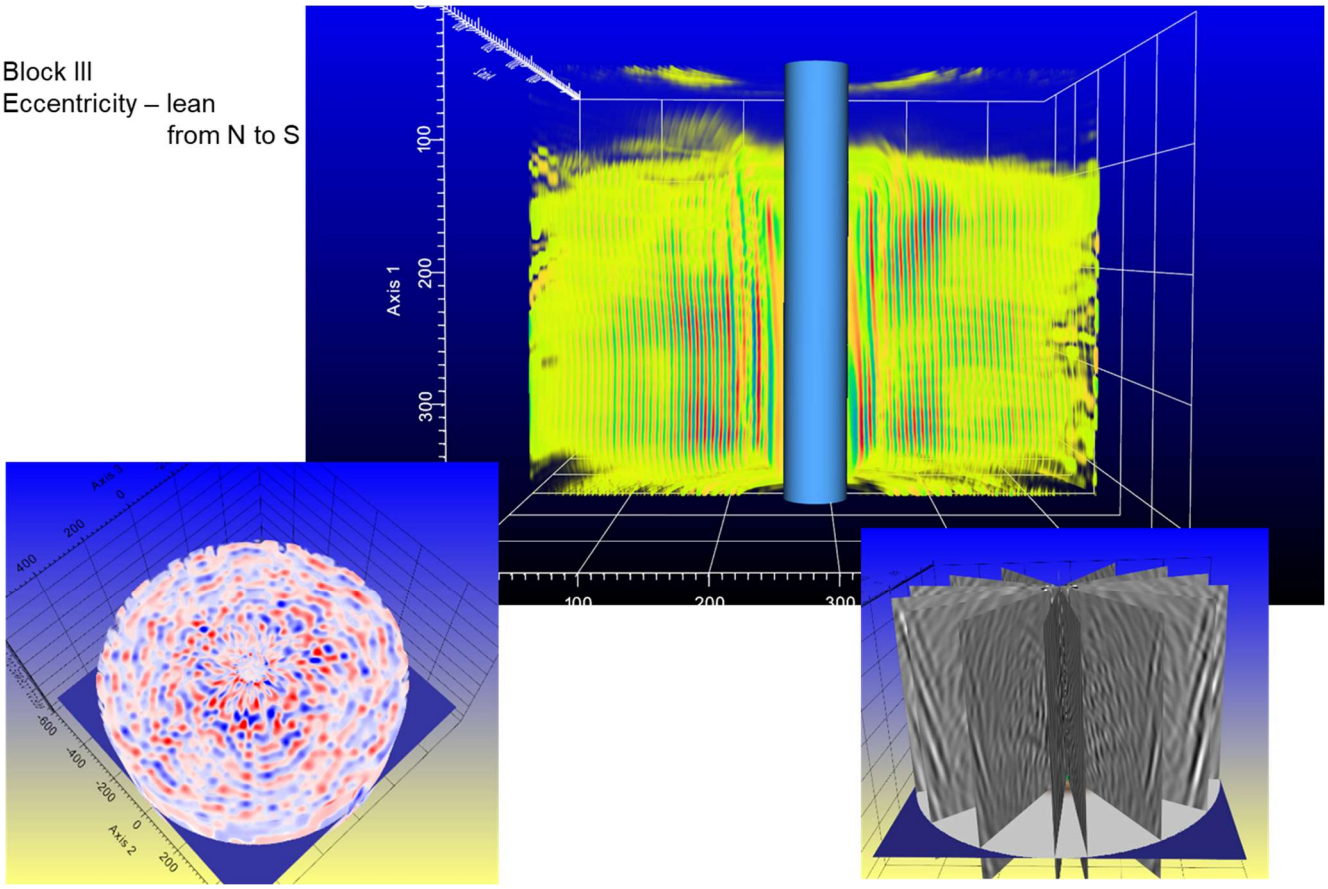

Figure 22. 3-dimensional visualization of a borehole in granite.

ORNL further developed their Model-Based Image Reconstruction (MBIR) approach to produce usable information on boreholes. The basic idea was to implement MBIR method for LANL high-power, highly-focused ultrasound system. MBIR is a technique mostly used for x-ray transmission imaging applications (e.g., microscopy, and computed tomography). MBIR is usually a linear method and includes mathematical models of application physics (e.g., model of sound waves generation at the transmitters, propagation of waves through the specimen, and sensing of reflected waves by receivers.), and statistical model of the expected reconstruction image intensity values and the relative differences between neighboring pixels.

In principle, MBIR should provide cleaner reconstructions relative to delay and sum approaches, such as Synthetic Aperture Focusing Technique (SAFT), faster reconstructions relative to non-linear techniques, requires minimum input data manipulation (e.g., truncation of signal, manual filtering), and the method can be combined with other state of the art techniques (e.g., Machine Learning) via plug-n-play techniques for even higher quality reconstructions.

Forward Model Parameters		
Parameter	**Value**	**Unit**
Number of rows	140	---
Number of columns	70	---
Reconstruction resolution	3	mm
Sampling frequency	2	MHz
FOV height	420	mm
FOV width	210	mm

Prior Model Parameters			
Parameter	**Value**	**Unit**	**Description**
σ	0.1	Pascal	Variance of y
m	0.01	-	A scalar for the variance of the image X for deeper regions
σ_0	10	m^{-3}	QGGMRF regularization parameter
a	5	-	---
p	1.1	-	---
q	2.0	-	---
T	1	-	---
No. of iterations	100	-	---

- In the forward model, the source is a linear-array tilted by 5 degree.

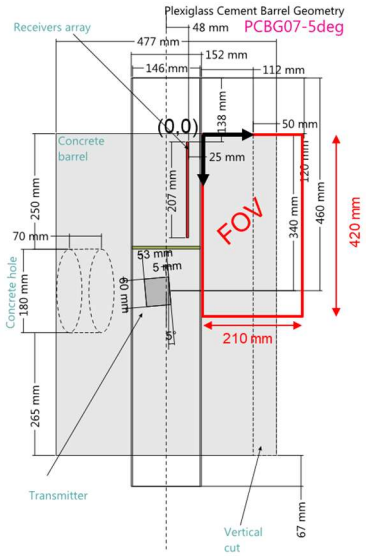

Figure 23. Forward & prior model parameters used for reconstruction.

The main goal of MBIR is to generate high-quality ultrasound images in near-real time for heterogenous specimens. The main challenge for MBIR method is related to the proper handling of strong reverberations due to high-intensity source beam.

In terms of work performed, the MBIR forward model has been modified to account for heterogenous media as in LANL experiment, linear-array source instead of a single point to consider the orientation of the source, extended field of view beyond the backwall, and identification of MBIR parameters configuration. Synthetic testing of MBIR method was performed, by modeling of LANL specimen and system on k-wave, and reconstructions of several modified specimens to validate results. Testing of MBIR method with real data showed results with the real data look very encouraging, and that more results needed to ensure proper operation and consistent results. Additionally, added source apodization to real beam profile.

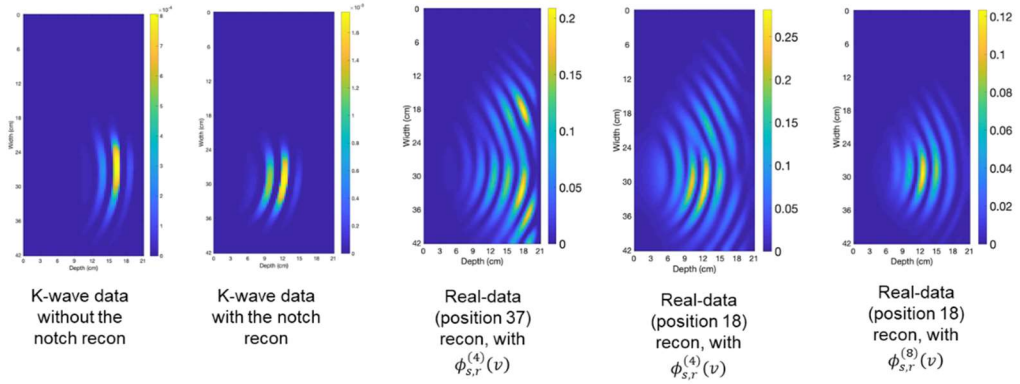

Figure 24. Forward & prior model parameters used for reconstruction.

Task 5. Technique refinement

1. **Planned Activities**:
   Refine the technique and enhance all detection algorithms.
2. **Actual Accomplishments**:
   Significantly improved techniques related to excitation of the acoustic source, receiving side, stepping in both vertical and azimuthal direction.

Task 6. Enhance capabilities for foamed cements

1. **Planned Activities**:
   Investigate and improve detection range through foamed cements.
2. **Actual Accomplishments**:
   The predicted Young's modulus and Poisson's ratio of the foamed cement presented here will be very useful for us to accurately predict the wave velocities in the foamed cement. Accurate wave velocity predictions are essential for the success of the 3D Acoustic Borehole Integrity Monitoring System. During the next phase, we will incorporate the material models in the simulation of the wave propagation in a well-bore model using the finite element program.
   Determined elastic properties of foamed cements for cylinder specimens with size approximately 25 mm (diameter) x 110 mm. Data are summarized in *Table 5*, below. Both compressional and shear sound speeds were determined. A graph of the change in elastic modulus with entrapped air is shown in Figure 25. A large change in elastic moduli is observed with air content, a clear indication of significant softening.
   Table 5. Elastic properties of foamed cements

Case (Foam Quality)	**0%**	**10%**	**20%**	**30%**
P-Wave Velocity^{+} ($^{m}/_{s}$)	3371.5	3060.4	2877.6	2661.8
Mass Density^{+} ($^{kg}/_{m3}$)	2120.9	1853.2	1650.3	1468.4
Poisson's Ratio*	0.18	0.18	0.19	0.2
Young's Modulus (GPa)	22.2	15.48	11.9	8.8

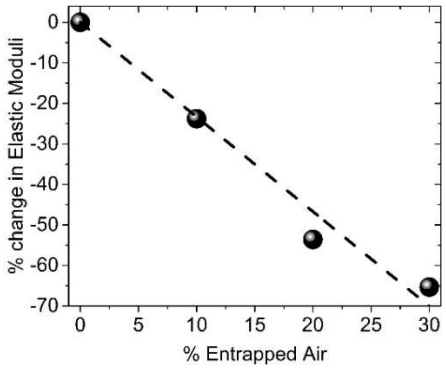

Figure 25. Percentile change of elastic moduli with entrapped air.

Investigated temperature dependence of sound speed of foam cements with temperature, up to depths in excess of 6 km (assuming a gradient of 25°C/km). A graph for 10% foamed cement is shown in Figure 26.

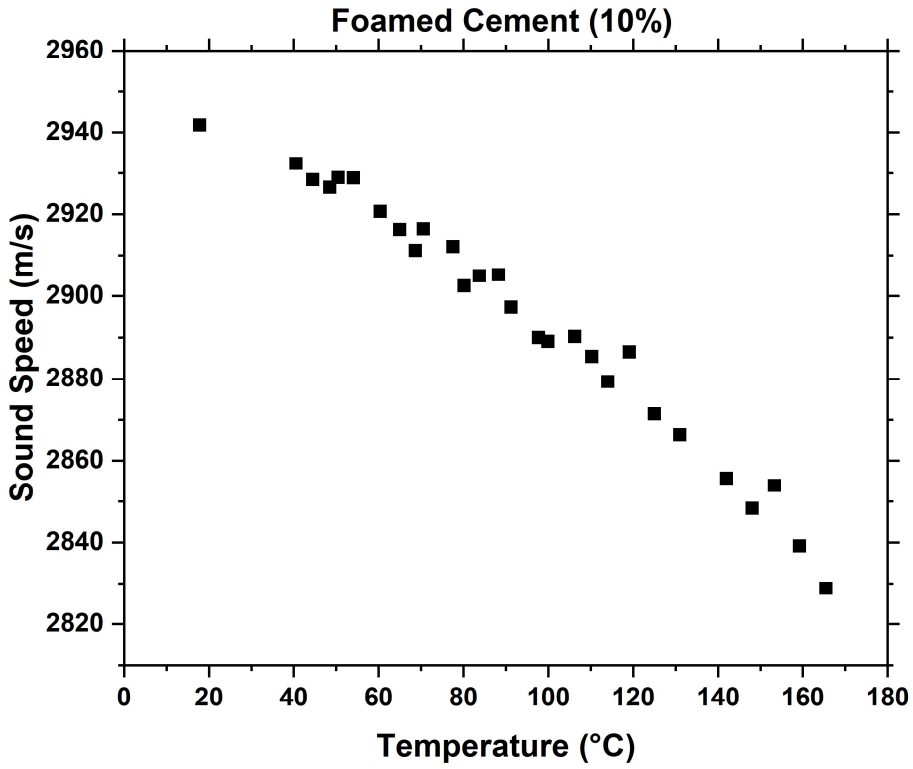

Figure 26. Compressional sound speed dependence with temperature.

Phase 4. Technology Development and Verification

Develop and refine a proof-of-principle prototype and test functionality in real wells.

Task 1. Prototype development

1. **Planned Activities**:
   Develop an engineering prototype. The prototype has to meet the standards required for CO_2 sequestration and geothermal industry, in terms of resistance to corrosion, high temperature and high pressure.
2. **Actual Accomplishments**:
   The acoustic source consists of a single Boston PiezoOptics PZT-5A, 1 MHz, 50 mm diameter piezoelectric transducer. The transducer is radially clamped by mounting it into a Plexiglas tube and affixing it to the tube walls using a Tungsten epoxy. A detailed drawing is shown in Figure 27 below.

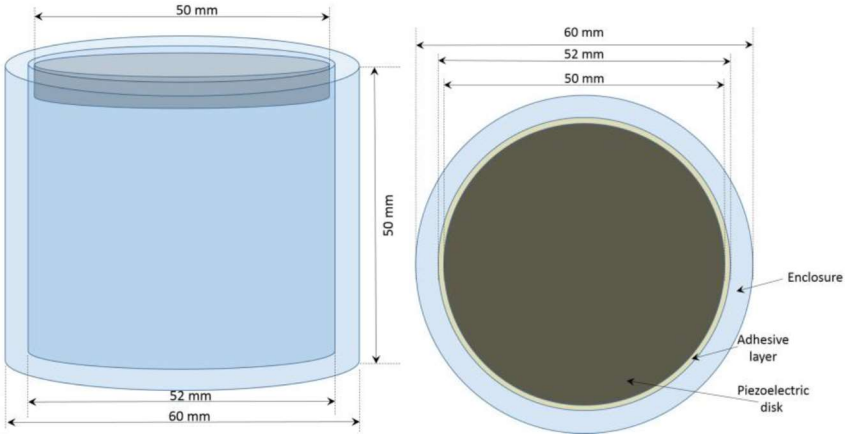

Figure 27. Drawing of the acoustic source.

The receiver array consists of 15 Boston PiezoOptics PZT-5A, 12.7 mm diameter, 500 kHz transducers that have been potted into a Plexiglas array at regular 15 mm inter-receiver distances, see Figure 28.

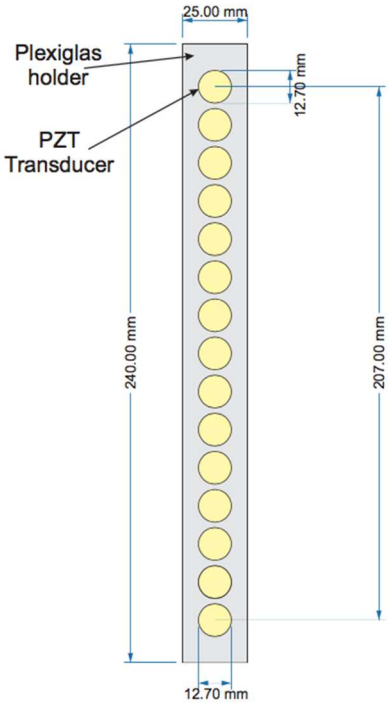

Figure 28. Drawing of the transducer array.

The transmitter is mounted below the receiver array in an assembly that allows for the transducer to be tilted at any desired angle relative to the receiver array. The transmitter and the receiver array are locked into a position such that the axis normal to their centers are always coplanar to each other. A detailed drawing, with dimensions, is shown in Figure 29.

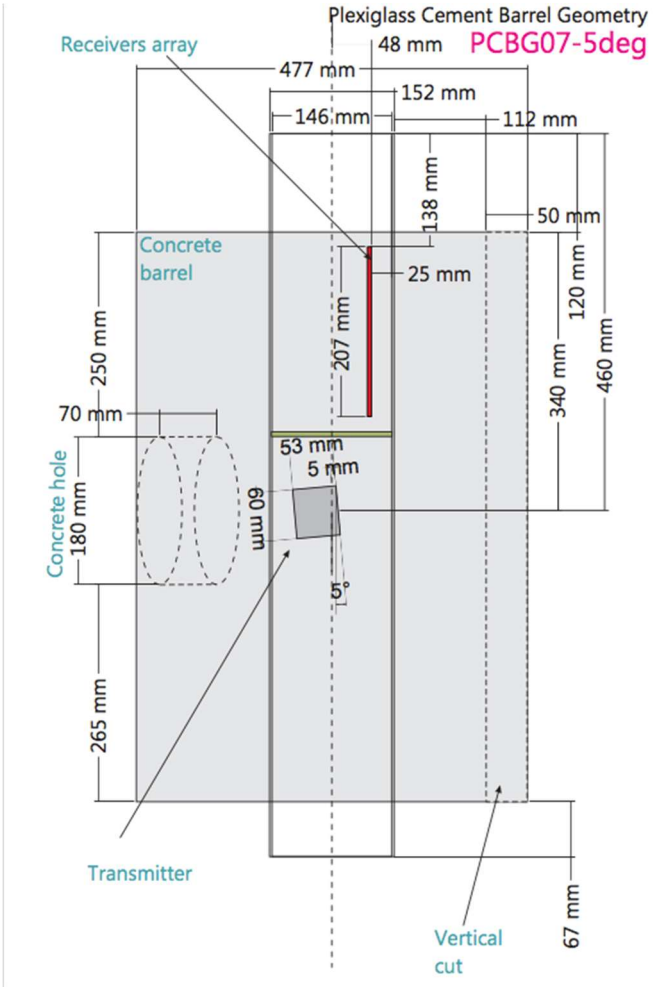

Figure 29. Drawing of the 3D Acoustic Borehole Integrity Monitoring System, as mounted in a concrete barrel with open borehole.

For laboratory testing, the complete system is mounted to a Velmex precision linear stage, for lowering down the borehole, as well as a Velmex precision rotating stage, for rotating it 360° inside the borehole at each depth. The transmitter is excited by a Tektronix Arbitrary Function Generator (AFG) 3102 using a fixed-frequency Tukey envelope at the resonant modes (radial modes) of the transmitter, identified by a Bode 100 Vector Network Analyzer (29 kHz, 42.4 kHz, 58 kHz, and 118.8 kHz). The pulse duration was 200 µs for the first two frequencies, and 50 µs for the second two, in order to ensure that at least 3 cycles were present in the pulse. The receivers were routed through a Keithley 7001 multiplexer and then into a Keithley 3940 Programmable Digital Filter which applied a bandpass of 25-350 kHz (Butterworth) and 40 dB gain. The signal was then digitized by a Tektronix Digital Phosphor Oscilloscope (DPO) 7054. Images of the clamped transmitter, as well as the completed system are shown below in Figure 30.

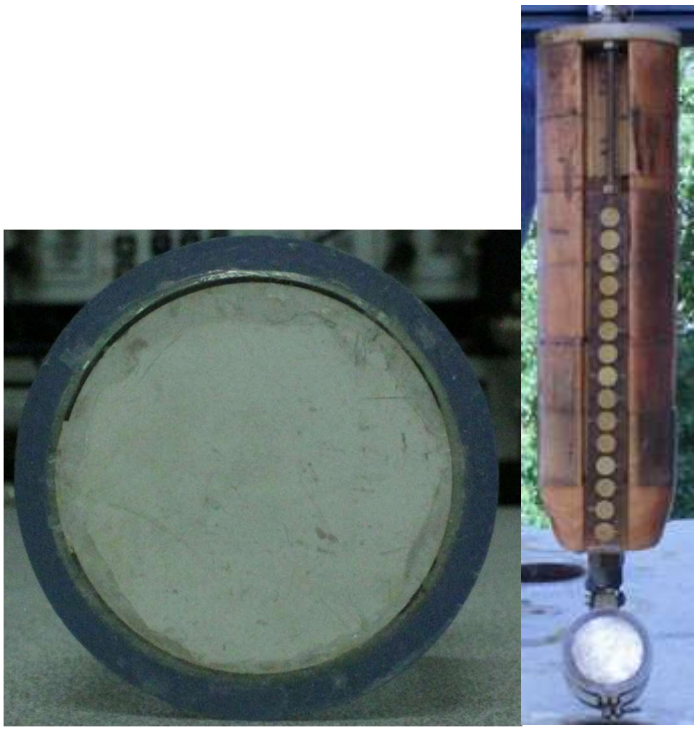

Figure 30. Illustration of the source and the receivers' array.

Task 2. Prototype verification at lab scale and in field

1. **Planned Activities**:
   Carry out extensive testing both in the lab and at other appropriate facilities.
2. **Actual Accomplishments**:
   Extensive testing was performed in: Plexiglas pipe embedded in concrete barrel, carbon steel pipe embedded in concrete barrel, Sierra White granite with steel pipe, and Mancos shale with steel pipe, with neat cement and foam cement, respectively. Some examples are shown in Figure 21, Figure 22, Figure 31 and Figure 32.

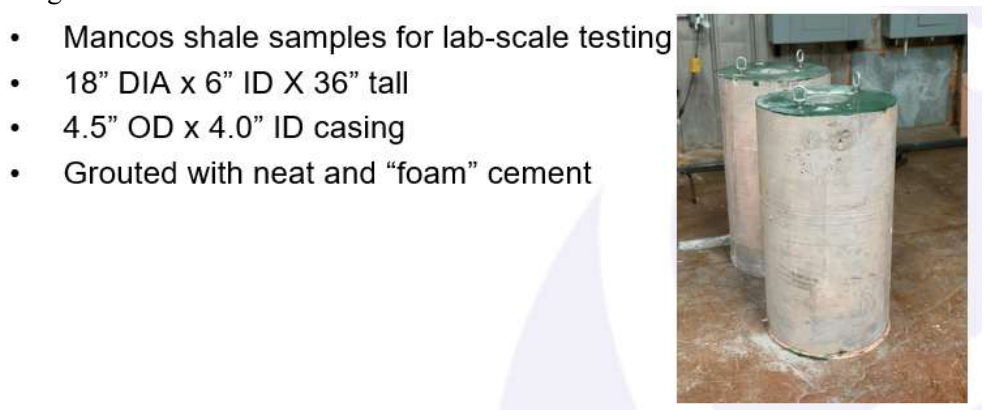

Figure 31. Mancos shale wellbores.

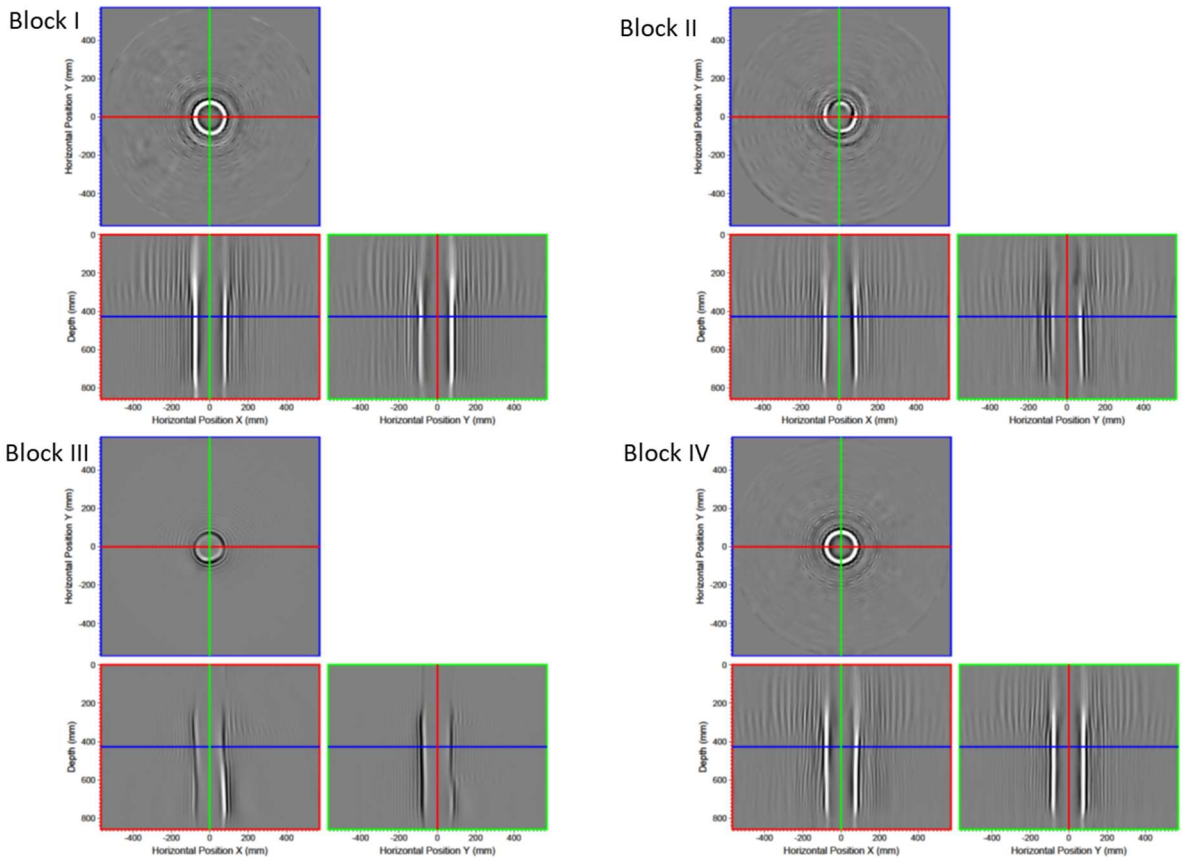

Figure 32. Example of imaging accomplished in simulated wellbores.

Task 3. Hardware/software enhancement and refinement

1. **Planned Activities**:
   Develop robust operation & analysis software, for near real-time 3D imaging by speeding up the measurement and analysis process.
2. **Actual Accomplishments**:
   Increased data collection speed by ~2 orders of magnitude, by using a shaped waveform with large bandwidth, Figure 33, and by using a highly customized multi-channel digitizer (National Instruments), with a specialized LabView software for data acquisition, Figure 34.

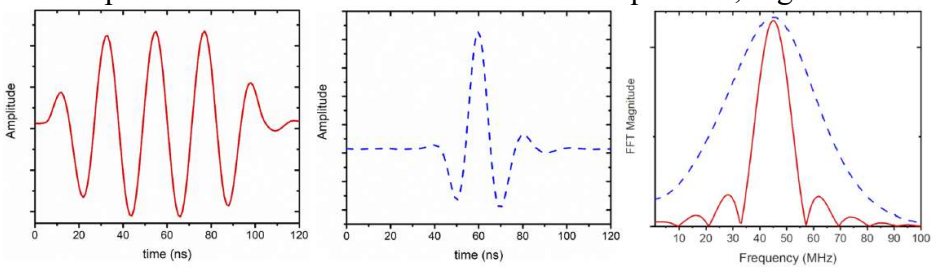

Figure 33. Shaped waveform used as excitation of the acoustic source.

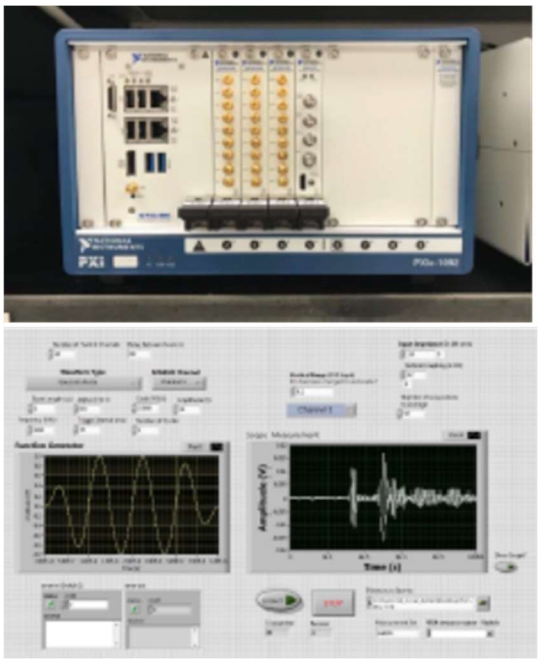

Figure 34. Hardware and software to control the system.

In parallel, significant efforts were directed towards improving the translational/rotational stage, such that data can be collected in a faster fashion, with increased resolution, and deeper penetration depth. This is summarized in Figure 35.

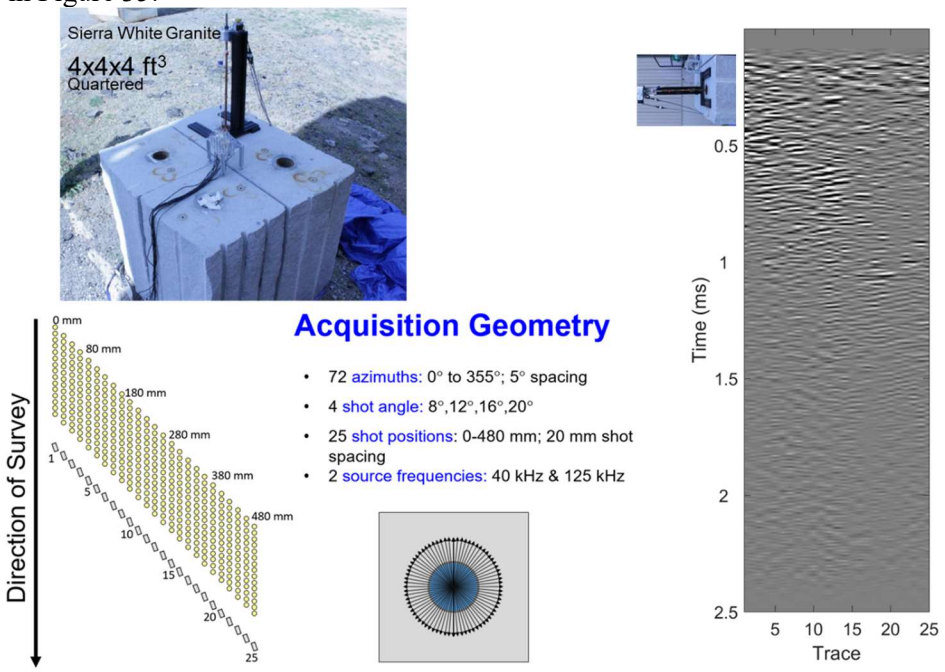

Figure 35. Snapshot of technique refinement.

PROJECT MANAGEMENT

Issues, Risks, and Mitigation (If Applicable): The COVID pandemic had a significant impact on experimental work. The following test borehole was drilled, but we did not get a chance to perform measurements:

- Drilled test borehole at New Mexico Tech
- Blue Canyon Dome in Socorro, NM
- 2" core to 30'
- 6.0" borehole to 30'
- 4.5" OD X 4.0" ID casing to 30'

Figure 36. Blue Canyon Dome in Socorro, NM

Changes in Approach (If Applicable): N/A

Key Personnel (If Applicable): N/A

Recipient Requests for DOE Attention (If Applicable): N/A

PROJECT OUTPUT

Publications (If Applicable):

1. On the Bandwidth and Beam Profile Characteristics of a Simple Low-Frequency Collimated Ultrasound Beam Source
   J. Greenhall, V.K. Chillara, D.N. Sinha, **C. Pantea**
   J. Vib. Acoust., vol. 143, No. 6, (2021), 064501.
2. On the in-plane vibrations and electromechanical resonance characteristics of non-uniformly polarized rectangular piezoelectric wafers: Selective mode-type excitation and specific mode enhancement
   V.K. Chillara, C. Hakoda, **C. Pantea**
   J. Sound Vib., vol. 506, (2021), 116129.
3. Noninvasive acoustic measurements in cylindrical shell containers
   J. Greenhall, C. Hakoda, E.S. Davis, V.K. Chillara, **C. Pantea**
   IEEE Trans. Ultrason., Ferroelect., Freq. Contr., vol. 68, No. 6, (2021), pp. 2251-2258.
4. A physics-based signal processing approach for noninvasive ultrasonic characterization of multiphase oil-water-gas flows in a pipe
   V.K. Chillara, B. Sturtevant, **C. Pantea,** D.N. Sinha
   IEEE Trans. Ultrason., Ferroelect., Freq. Contr., vol. 68, No. 4, (2021), pp. 1328-1346.
5. The effect of a transducer's spatial averaging on an elastodynamic guided wave's wavenumber spectrum
   C. Hakoda, V.K. Chillara, **C. Pantea**
   Ultrasonics, vol. 114, (2021), 106422.
6. Multi-level information storage using engineered electromechanical resonances of piezoelectric wafers: A concept piezoelectric quick response (PQR) code
   C. Hakoda, E.S. Davis, **C. Pantea**, V.K. Chillara
   Sensors, 20(21), (2020), pp. 1-7, 6344.
7. A broadband wavelet implementation for rapid ultrasound pulse-echo time-of-flight measurements
   B.T. Sturtevant, N. Velisavljevic, D.N. Sinha, Y. Kono, **C. Pantea**
   Rev. Sci. Instrum., vol. 91, (2020), 075115.
8. Ultrasonic waves from radial mode excitation of a piezoelectric disc on the surface of an elastic solid
   V.K. Chillara, J. Greenhall, **C. Pantea**
   Smart Mater. Struct., vol. 29, (2020), 085002.
9. Nonlinear acoustic crack detection in thermoelectric wafers
   J. Greenhall, S. Grutzik, A. Graham, D.N. Sinha, **C. Pantea**
   Mechanical Systems and Signal Processing, vol. 139, no.5, (2020), 106598.
10. Ultrasonic Bessel beam generation from radial modes of piezoelectric discs
    V.K. Chillara, E.S. Davis, **C. Pantea**, D.N. Sinha
    Ultrasonics, vol. 96, no. 7, (2019), pp. 140-148.
11. Full-waveform inversion and least-squares reverse-time migration imaging of collimated ultrasonic-beam data for high-resolution wellbore integrity monitoring

Y. Chen, K. Gao, E.S. Davis, D.N. Sinha, **C. Pantea**, L. Huang
Appl. Phys. Lett., vol. 131, issue 7, (2018), 071903.

12. Radial modes of laterally stiffened piezoelectric disc transducers for ultrasonic collimated beam generation
    V.K. Chillara, **C. Pantea**, D.N. Sinha
    Wave Motion, vol. 76, (2018), pp. 19-27.
13. Low-frequency ultrasonic Bessel-like collimated beam generation from radial modes of piezoelectric transducers
    V.K. Chillara, **C. Pantea**, D.N. Sinha
    Appl. Phys. Lett., vol. 110, issue 6, (2017), 064101.
14. Beam Profile Characterization for Thickness Mode Transducers versus Radial Modes
    E. S. Davis, V. Chillara, C. Chavez, D. N. Sinha and **C. Pantea**
    2019 IEEE International Ultrasonics Symposium (IUS), Glasgow, United Kingdom, 2019, pp. 1663-1665
15. Development of a 3D Acoustic Borehole Integrity Monitoring System
    C. Chavez, E. S. Davis, V. Chillara, D. N. Sinha and **C. Pantea**
    2019 IEEE International Ultrasonics Symposium (IUS), Glasgow, United Kingdom, 2019, pp. 1666-1669
16. Collimated acoustic beams from radial modes of piezoelectric disc transducers
    V.K. Chillara, E.S. Davis, **C. Pantea** and D.N. Sinha
    AIP Conf. Proc., vol. 2102, (2019), pp. 040013.

Technologies/Techniques (If Applicable): The main focus of this project is the development of a unique acoustic source that consists of a collimated beam of low frequency, with a bandwidth between 10 and 150 kHz. The source will be able to rotate azimuthally for 360 deg, move vertically along the borehole, and vary angle of incident beam with respect to borehole axis, such that the environment around the borehole is fully investigated. The acoustic source, incorporated in a logging tool, equipped with appropriate receivers, can provide information in several areas: mapping of the borehole shape and borehole casing, cement bond quality logging, mapping of the area around the borehole, fault detection, fracture detection, porosity mapping, fluid saturation mapping, fluid flow paths, etc.

Status Reports (If Applicable): N/A

Media Reports (If Applicable):

- LANL Faces Of Innovation: Cristian Pantea, Acoustic Scientist
  https://losalamosreporter.com/2019/06/10/lanl-faces-of-innovation-cristian-pantea-acoustic-scientist/
- LANL Institutional video on Acoustic Collimated Beam (ACCObeam)
  https://www.youtube.com/watch?v=qzaPYDWXLbE&feature=youtu.be
- LANL Science Highlights
  https://www.lanl.gov/science-innovation/science-highlights/2018/2018-09.php

- Santa Fe New Mexican: Using sound to 'see' through solid objects https://www.santafenewmexican.com/news/health_and_science/using-sound-to-see-through-solid-objects/article_a1c03aa7-d9eb-5db6-88ec-fba838b2d859.html
- Los Alamos Daily Post: LANL High-Impact Los Alamos Innovations Honored As R&D 100 Award Finalists https://ladailypost.com/lanl-high-impact-los-alamos-innovations-honored-as-rd-100-award-finalists/
- Machine Design: Simple Device Takes Imaging with Sound to a New Level https://www.machinedesign.com/community/simple-device-takes-imaging-sound-new-level
- LANL: High-impact Los Alamos innovations honored as R&D 100 award finalist https://www.lanl.gov/discover/news-release-archive/2018/August/0827-rd-100-finalists.php

Invention Disclosures (If Applicable): disclosures on receiver's array and tool ruggedization for challenging conditions.

Patent Applications (If Applicable): submitted patent on low-frequency collimated acoustic source: SIMPLE BESSEL-LIKE COLLIMATED SOUND BEAM GENERATOR

Licensed Technologies (If Applicable): N/A

Networks/Collaborations Fostered (If Applicable): ORNL, SNL, NETL, Univ of West Virginia.

Websites Featuring Project Work or Results (If Applicable):

- LANL Institutional video on Acoustic Collimated Beam (ACCObeam) https://www.youtube.com/watch?v=qzaPYDWXLbE&feature=youtu.be

Other Products (If Applicable): N/A

Awards, Prizes, and Recognition (If Applicable):

- Induction into the inaugural class of Los Alamos National Laboratory's Innovation Society, Feynman Center for Innovation (FCI), 2018
- Finalist of 2018 R&D100 Awards, with *ACCObeam: Acoustic Collimated Beam*

REFERENCES

Davatzes, N.C. and Hickman, S., 2005. Comparison of acoustic and electrical image logs from the Coso geothermal field, CA. In Proceedings, Thirtieth Workshop on Geothermal Reservoir Engineering, Stanford University (pp. 1-11).

Massiot, C., D.D. McNamara, A. Nicol, J. Townend, 2015. Fracture width and spacing distributions from borehole televiewer logs and cores in the Rotokawa Geothermal Field, New Zealand. Proceedings World Geothermal Congress 2015, Melbourne, Australia, 19–25 April 2015.

Prensky, S. 1999. Advances in Borehole Imaging Technology and Applications. In Borehole Imaging: Applications and Case Histories, ed. M. Lovell, G. Williamson, and P. Harvey, 159, 1-43. London: Geological Soc. Special Publications.

Zemanek, J., Glenn, E.E., Norton, L.J. et al. 1970. Formation evaluation by inspection with the borehole televiewer. Geophysics 35 (2): 254–269. http://dx.doi.org/10.1190/1.1440089.

Gao, K., B. Chi, and L. Huang, *Elastic least-squares reverse-time migration with implicit wavefield separation.* Expanded Abstract submitted to 2017 SEG Annual Meeting, 2017.

Chi, B., K. Gao, and L. Huang, *Least-squares reverse-time migration guided full-waveform inversion.* Expanded Abstract submitted to 2017 SEG Annual Meeting, 2017.

Almansouri, H., et al., *Progress implementing a model-based iterative reconstruction algorithm for ultrasound imaging of thick concrete.* AIP Conference Proceedings, 2017. **1806**(1): p. 020016.

Crandall, D., et al., *Foamed Cement Analysis With Computed Tomography.* 2014(46230): p. V01CT25A002.

Jacobs, T., *Offshore Industry Gets a Fresh Look at Foamed Cement.*

Kutchko, B., et al., *Assessment of Foamed Cement Used in Deep Offshore Wells*. Society of Petroleum Engineers.

APPENDIX A – Tools available on the market

Technique	Company	Range	Frequency	Resolution	Notes
FMI – Fullbore Formation Microimager	Schlumberger	30 inches	N/A	5 mm both	Temp 175 C/pressure 20 ksi/ 80% of borehole in 8 inch hole coverage
IBC – Imaging Behind Casing	Schlumberger	Casing-formation interface	~200 kHz	102 mm vert 30 mm azim	Good for low-impedance cements/ produces SLG maps / can possibly see casing position within borehole
CBL – Cement Bond Log (multiple tools)	Schlumberger	Casing-cement interface	20 kHz	Poor - ~.91m	Mostly for evaluation of cement-casing interface/ 260 C / 30 ksi
USI – Ultrasonic Imager	Schlumberger	Casing-cement interface	200 – 700 kHz	30 mm lateral[2] 15.24 cm vert	177 C/ 20 ksi
UBI – Ultrasonic Borehole Imager	Schlumberger	Full Borehole, all standard sizes	250, 500 kHz	"high"	Not influenced by mud type, advanced software
OBMI – Oil-Based MicroImager	Schlumberger	3.5 in	N/A	Features as small as 1 cm	Microresistivity imaging in nonconductive oil-based systems
ARI – Azimuthal Resistivity Imager	Schlumberger	~100 in?	N/A	8 inches vert/ 60° azim angle for 1 inch standoff	177 C/ 20 ksi/ resistivity
AIT - Array Induction Imager Tools (multiple)	Schlumberger	10-90 in	N/A	.61m or .30m smooth borehole	125 C- 260 C/ 15 – 30 ksi/ 3600 feet per hour log speed/ resistivity
Isolation Scanner Tool	Schlumberger	Casing and	~200kHz	1.52 cm vert	177 C/ 20 ksi/ 563 feet per hour log speed

		annulus up to 3 in			
Sonic Scanner	Schlumberger	formation	wide	<1.82 m	177 C/ 20 ksi
XMAC F1	Baker Hughes	100 feet	Low frequency dipole source	low	232 C/ 30 ksi/ 50 feet per minute log speed/ 4.5 in minimum borehole size/ features don't need to intercept borehole
Array Dielectric eXplorer formation evaluation service	Baker Hughes	6 in	N/A ("multiple")	3 in	150 C/ 20 ksi/ Mostly for determining mobility of oils and porosity values as well as hydrocarbon saturation/ Acquires permittivity and conductivity data/ 5.875 inch min borehole diameter
High-Resolution Vertilog	Baker Hughes	5.3 in to 9.425 in depending on hole diam (casing tool)	N/A	?	175 C/ 15 ksi/ Uses Hall effect sensors for magnetic flux leakage detection/ has minimum operating distance from tool
Digital Magnelog (DMAG)	Baker Hughes	Casing	multi	?	Designed to detect wall thickness changes by measuring magnetic field shift
Acoustic Cement Bond Log	Baker Hughes	Casing-Cement Interface	?	?	177 C/ 17 ksi/ 2.38 in min casing
Imaging Caliper Log	Baker Hughes	Casing	N/A (mechanical)	.003 in azim .14 in vertical at	150 C/ 15 ksi/ resolution strongly dependent on borehole size. Listed resolution is best, worst is .013 in

				$11\frac{11}{16}$ in casing	azim, .28 in vertical when casing is 8 inches.
Segmented Bond Tool (SBT)	Baker Hughes	Casing-Cement interface	Ultrasonic range	3 in vertical	177 C/ 20 ksi/ Insensitive to heavy borehole fluids and moderate tool eccentering
Radial Analysis Bond Log (RAL)	Baker Hughes	Casing-Cement Interface	?	Similar to other CBL	177 C/ 20 ksi/ can detect microannulus
Integrity eXplorer Cement Evaluation	Baker Hughes	Casing-Cement Interface	?	?	177 C/ 20 ksi/ electromagnetic-acoustic transducer sensor/ the service can provide measurements in air-filled boreholes and gas-cut mud systems/ 4.5 in minimum casing size
STAR Imager	Baker Hughes	Into Reservoir ?	N/A	.2 inch both	177 C/ 20 ksi/ Conductive mud only, resistivity imaging/ 6 in min borehole/ EARTH imager does oil-based muds
Circumferential Borehole Imaging Log	Baker Hughes	?	250 kHz	?	3.625 in diameter tool/ https://www.bakerhughes.com/products-and-services/evaluation/openhole-wireline-services/geology/circumferential-borehole-imaging-log
UltrasonicXplorer Imaging Service	Baker Hughes	?	250 kHz	"high"	177 C/ 20 ksi/ 4.5 in min borehole size
GeoXplorer Imaging Service	Baker Hughes	Near-wellbore	N/A	.8 in vert .3 in azim	177 C/ 25 ksi/ Nonconductive mud

					systems/ 7 in min borehole/ 79% in an 8-in. (203-mm) borehole coverage
Wellbore Geometry Instrument (WGI) Measurement Service	Baker Hughes	Casing only	N/A	1 in vert	
MR eXplorer	Baker Hughes	2.1-3.8 in	~500-1000 kHz (magnetic resonance)	high	175 C/ 20 ksi/5.875 in min borehole size/ Targeted towards permeability and porosity measurements and characterize oil
Circumferential Acoustic Scanning Tool (CAST)	Halliburton	Casing and Cement	?	1.8° azim openhole 3.6° casedhole, .3 in vert	175 C/ 20 ksi/ 5 in borehole min/ DeepSuite CAST-XR 35 ksi
Multifinger Imaging Tool (MIT)	Halliburton	Casing	N/A	?	177 C/ 20 ksi/ resolution similar to competitors, completely mechanical
Acoustic Conformance Xaminer® (ACX™)	Halliburton	Casing and Cement?	?	high	Used to triangulate leak sources
Electromagnetic Pipe Xaminer® V (EPX™ V) Tool	Halliburton	Casing only	N/A	.015 inch accuracy defect detection	177 C/ 15 ksi/ Used exclusively to characterize extent of damage in casing after already being picked up by another method
Xaminer® Sonic Imager Service (also Full Wave	Halliburton	formation	low?	Low?	177 C/ 20 ksi/ Measures formation p-wave velocity using farthest-spaced monopole/

Sonic Tool (FWS))					Mostly measures slowness
Radial Cement Bond Log (RCBL™)	Halliburton	Cement-Formation Interface	?	?	Similar capabilities to other CBL tools
SPACE Panorama	Archer	Casing	3.5 MHz	.39 in vert 1.25° azim	150 C/ 15 ksi
ABI-40 Televiewer/ WellCAD	Advance Logic Technology	2" to 20" diameter depending on mud conditions	~1.2MHz	Caliper Resolution: 0.08 mm	Logging Speed: 3 to 24 ft/min Samples/revolution: up to 360

APPENDIX B – Comparison Matrix

Parameter	ACCObeam	Standard borehole sonic probe, e.g. BARS SCHLUMBERGER	Ultrasonic probe, e.g. UBI SCHLUMBERGER	SPACE Panorama ARCHER
Frequency	10-250 kHz	0.3-8 kHz	250, or 500 kHz	3.5 MHz
Comments: Low frequency is needed for deeper penetration, but conventional low-frequency sources have a very large beam spread, which decreases resolution. Our approach provides a low-frequency beam that is still collimated and has no side lobes.				
Penetration Range	3 m	15 m	Casing (< 10 mm)	Casing only
Comments: ACCObeam is collimated and has a much longer investigation range than other high-frequency sources, which leads to good understanding of both the borehole and the surrounding environment. Although it does not currently penetrate as far as standard probes, ACCObeam's collimation means that it surpasses standard probes in critical ways, namely imaging resolution (ACCObeam's resolution is 60-100 times better than standard sonic probes) and power efficiency. ACCObeam is also adaptable for numerous other applications.				
Resolution	3-5 mm	300 mm	4-5 mm	10 mm
Comments: ACCObeam has the deep penetration advantage of a low-frequency source, but it maintains the same resolution as higher-frequency sources. This resolution is critical because even small fractures, delaminations, and other defects can lead to catastrophic failure of a borehole.				
Collimation	< 6 deg	Monopole/dipole >180 deg	< 15 deg	< 6 deg
Comments: Our source has a very similar collimation/beam spread as its high-frequency competitors, even though it generates a low-frequency beam that penetrates much deeper than any high-frequency source. Please note the huge difference when compared with the standard borehole sonic probe.				
Cost	$	$$$$	$$$$	$$$$
Comments: All other products are offered as a service/package operated by a specific company, so the cost of using their source is thousands of dollars. ACCObeam costs $50-$200 to manufacture and is compatible with virtually any imaging software or hardware.				
Imaging through highly attenuating materials	Y	Y	N	N

Comments: The only other product able to image clearly and beyond casing in highly attenuating media (such as concrete, drilling mud, rock, and bone) is the low-frequency standard borehole sonic probe. However, standard probes have an extremely low spatial resolution and can miss important small features. On the other hand, our source works well in highly attenuating media while maintaining the resolution characteristic of high frequency.				
Parameter	**Your product**	**Standard borehole sonic probe, e.g. BARS** **Schlumberger**	**Ultrasonic probe, e.g. UBI** **Schlumberger**	**SPACE Panorama** **Archer**
Size	Small/compact	Large	Small/compact	Small/compact
Comments: ACCObeam is similar in size to high-frequency sources, but much smaller than a typical low-frequency source.				
Collimated beam at multiple frequencies	Y (several)	N	N	N
Comments: The UBI ultrasonic probe can provide either a somewhat collimated 250 kHz beam or a more collimated 500 kHz beam, but our source images at numerous frequencies ranging from 10–250 kHz while maintaining a tight collimation.				
Simple manufacturing process	Y	N	N	N
Comments: ACCObeam's design requires radial clamping, achieved by gluing a piezoelectric transducer into casing made of any strong material. Comparative technologies require filler material and a small matching inductor for "loading" the back of the transducer, making the packaging process more sophisticated.				
Images through various media	Y	N	N	N
Comments: No competing source can be used to image in assorted media. Since our source operates at a low frequency, it can transmit or receive in liquids, solids, gases, and air.				
Frequency hopping	Y	N	Y (limited)	N
Comments: ACCObeam supports as many as 4-10 frequencies, while the UBI has only two selectable frequencies.				

APPENDIX C – Prediction of Foamed Cement Material Properties

A material model has been developed to compute the degree of hydration of Class H cement using the chemical composition from the Mill Test Report shown in Table 1. The percentages of the four major compounds of cement (C_3S, C_2S, C_3A, C_4AF) can be estimated based on Bogue's equations.

Table 1: Chemical Compositions of Class H Cement

Components	CaO	SiO_2	Al_2O_3	Fe_2O_3	MgO	SO_3	Blaine (m^2/kg)	C_3S	C_2S	C_3A	C_4AF
%	64.7	22.3	2.6	4.3	2.3	2.9	310	61.7	17.3	0	12.7

The ultimate heat of hydration for the Class H cement calculated based on the formula by Lerch and Bogue (Eq.1) can be estimated to be about 481.14 J per gram of cement.

$$H_{ultimate} = 500 \cdot p_{C_3S} + 260 \cdot p_{C_2S} + 866 \cdot p_{C_3A} + 420 \cdot p_{C_4AF} + 624 \cdot p_{SO_3} + 1186 \cdot p_{FreeCaO} + 850 \cdot p_{MgO} \quad (1)$$

The isothermal calorimetry tests on the Class H cement samples were conducted to measure the early age heat of hydration of the Class H cement under a curing temperature of 23°C. A water- cement ratio (w/c) of 0.38 was used to prepare the specimens. A total of four specimens were prepared and tested in four separate channels. The average experimental heat generation and accumulated heat release of all the channels are shown in Figure 1 and Figure 2.

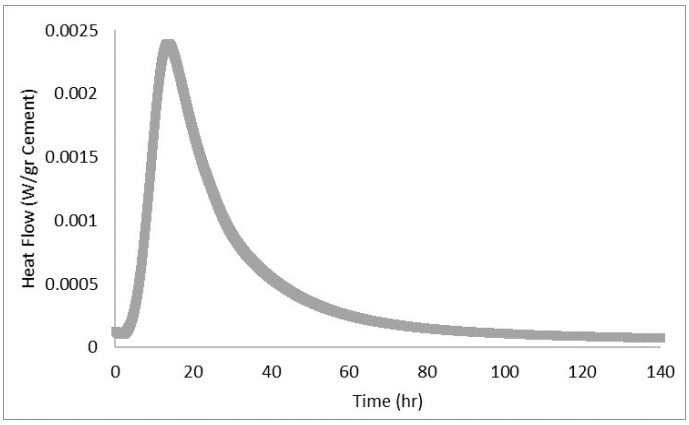

Figure 1: Heat generation of Class H cement at 23° C

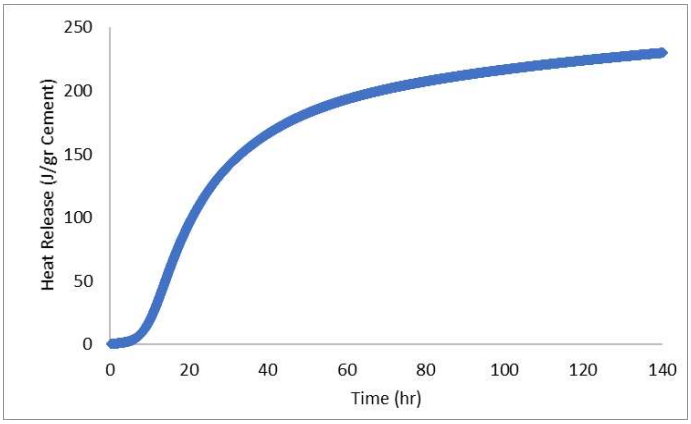

Figure 2: Accumulated heat release of Class H cement at 23 °C

The early-age degree of hydration was calculated using the experimental accumulated heat release and the ultimate heat generation with the following equation.

$$\alpha = \frac{H(t)}{H_u}$$

Where α is the degree of hydration, $H(t)$ is the heat release vs. time and H_u is the ultimate heat of hydration. The calculated degree of hydration is shown in Figure 3.

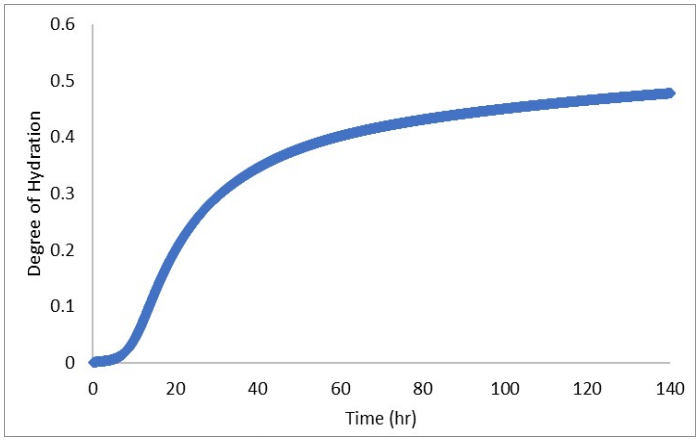

Figure 3: Degree of hydration of Class H cement

A material model computation based on Maekawa's multi-component model (2009) has been developed to calculate the accumulated heat generation of the cement paste based on its compound properties (C_3S, C_2S, C_3A, C_4AF). In this model the heat generation of each compound was calculated first, then the heat generations are summed to calculate the heat production of the whole cement mix.

The isothermal calorimetry experimental results and the results from a NIST model calculated based on the chemical compositions (Table 1) were used to calculate the degree of hydration and compared to the analytical results from the current material model (shown in Figure 4). The current model matches well with the NIST model but is slightly higher than the experimental results. Since both prediction models are very sensitive to the chemical characteristics of the cement, and the chemical composition used in the model was obtained from the Mill Test Report provided by the cement producer, which may not be identical to the cement sample under testing, once the chemical composition of the cement can be accurately determined (using X-Ray Diffraction or SEM analysis), the overall comparison can be improved.

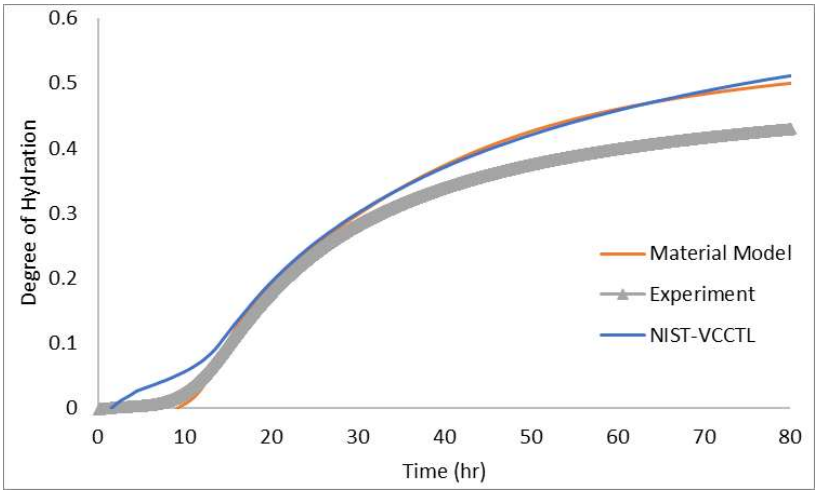

Figure 4: Comparison of the degree of hydration

The early-age Young's modulus of the neat Class H cement was measured using the ultrasonic pulse velocity (UPV) method. The material model was used to calculate

Young's modulus of the neat Class H cement, which is shown in Figure 5. Also, Figure 6 indicates the effect of having various water-cement ratios ranging from 0.37 to 0.40. The effective medium theory is the basis for the calculation of Young's modulus which assumes the cement paste is a porous medium consisting of hydration products (C-S-H gel), pores, pore water, and anhydrous cement. The results show that the increase of the water-cement ratio will reduce the modulus of elasticity. Figure 7 shows a typical nonlinear relationship between the Young's modulus of neat Class H cement and the w/c ratio (from 0.35 to 0.45). The relationship can be fitted using a second order polynomial function. This simple polynomial relationship can now be used to predict the Young's modulus of the neat Class H cement paste at the age of 28 days.

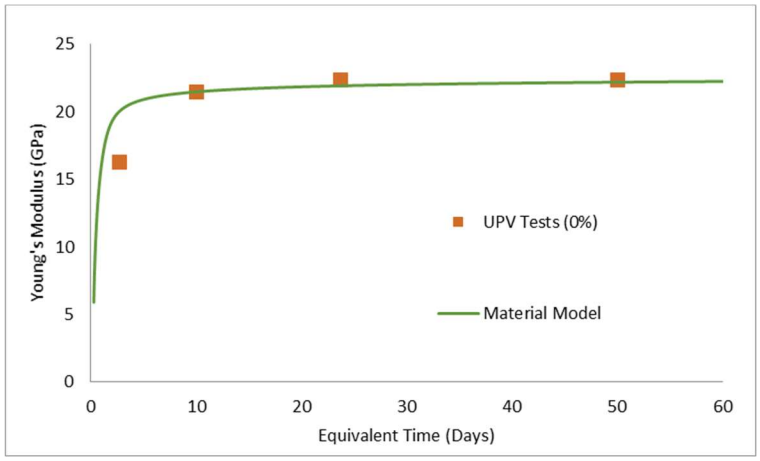

Figure 5: Young's modulus of neat (0%) Class H cement comparison (w/c = 0.38)

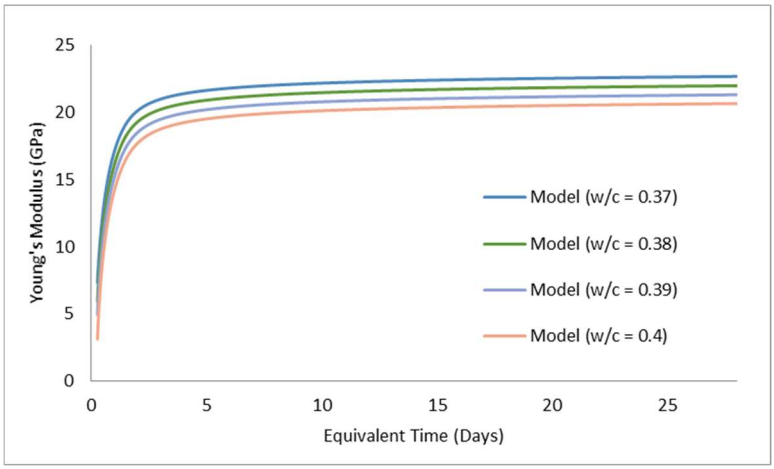

Figure 6: Effect of w/c ratio on Young's modulus of neat Class H cement

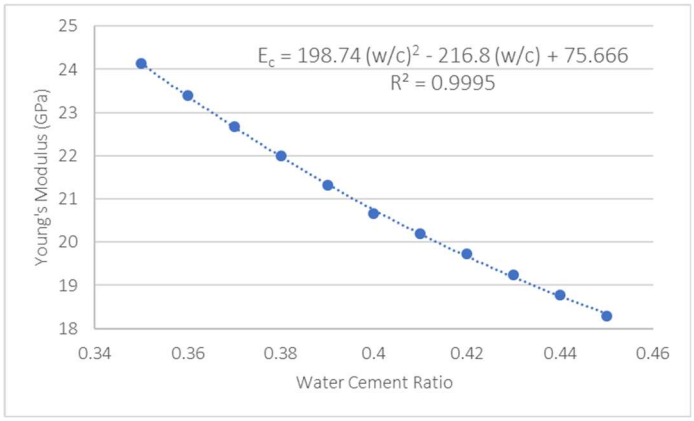

Figure 7: Young's modulus vs. w/c ratio of neat Class H cement at 28 days

The experimental heat measurements, from Pang et. al. (2013), for a few types of oil well cements (A, C, G, H-P, H-I, H-II) were compared to the results of our current material model. Table 2 shows the chemical compounds of all the types of cements determined by Bogue's method from Pang et. al. (2013). Pang et al. used isothermal calorimetry test to measure the hydration kinetics and estimate the degree of hydration at different curing temperature and pressure. The water-cement ratios used for the isothermal samples were 0.46, 0.56, 0.44, 0.38, 0.38, 0.38 for the A, C, G, H-P, H-I, H-II types cement, respectively. The current material model was used to calculate the heat of hydration and hydration kinetic. The results were compared to the digitized data obtained from the figures shown in the publication by Pang et al. The comparison is shown in Figure 8. Overall, the current material model seems to be able to have reasonable simulations of the heat generation for the various types of cement with different chemical compositions.

Table 2: Chemical compound percentages (Data from Pang et al., 2013)

Cement Type	**C_3S**	**C_2S**	**C_3A**	**C_4AF**	**w/c ratio**
A	61.7	12	8.4	9.4	0.46
C	72.2	5.2	2.2	11.8	0.56
G	62.6	15.9	4.8	10.9	0.44
H-P	47.9	27.5	0	16.2	0.38
H-I	66.5	11.7	0.3	13.4	0.38
H-II	71.6	7.4	0	12.8	0.38

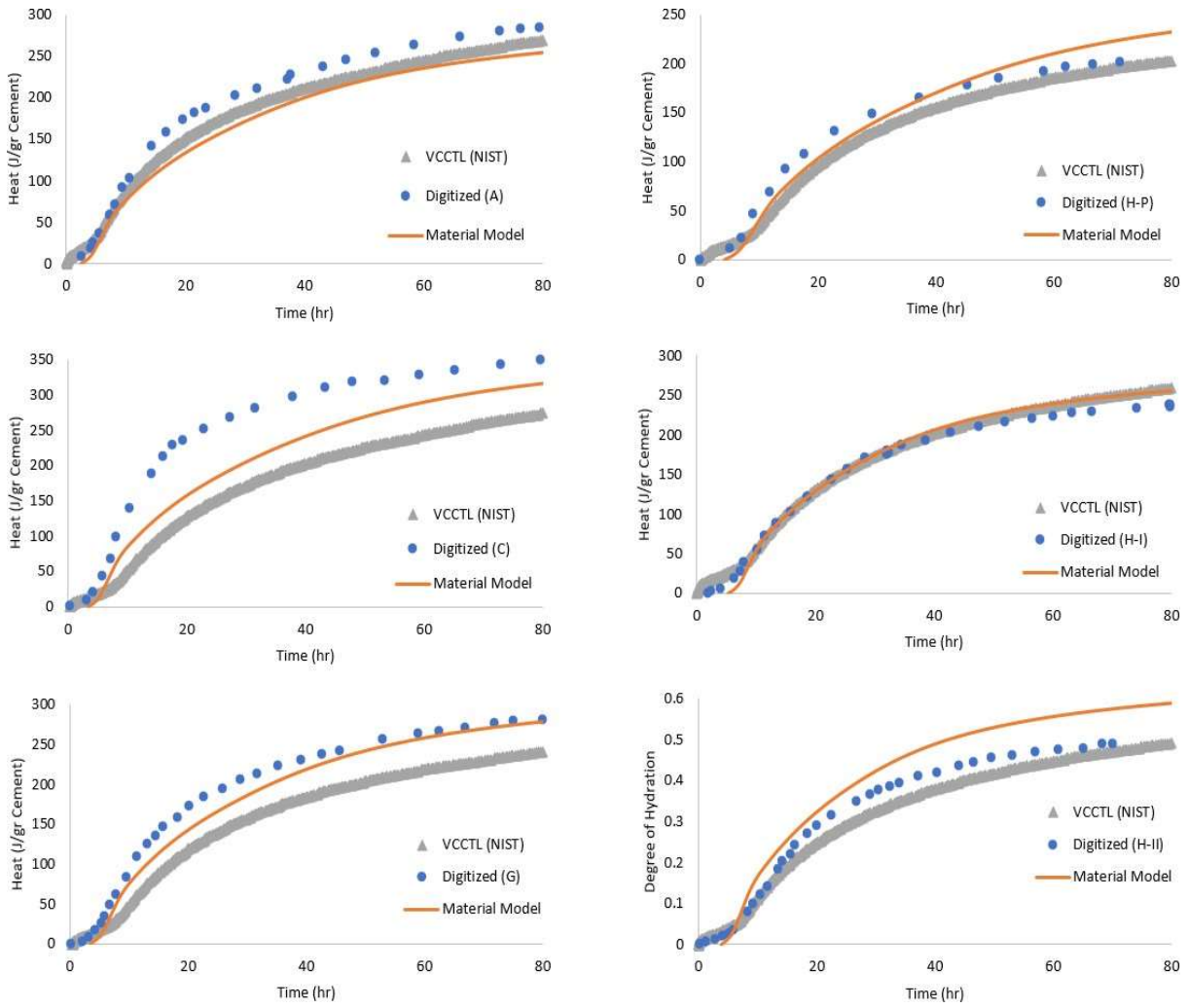

Figure 8: Heat release from different oil-well cements (experimental results from Pang et al., 2013)

Class H Cement with Different Foam Qualities

Two Lafarge Class H cement (Joppa Plant) buckets produced in September 2018, as well as 15 ml of FAW-20 (foaming agent), were collected for additional testing. These include the effects of different foam qualities on hydration kinetics. The chemical properties of the new cement received were compared to the previous one in Table 3 which were obtained from the Mill Test Report.

Table 3: Chemical compositions of Class H cement from the Mill Test Report

Product	CaO	SiO_2	Al_2O_3	Fe_2O_3	MgO	SO_3	Blaine (m^2/kg)	C_3S	C_2S	C_3A	C_4AF
OCT 2016	64.7	22.3	2.6	4.3	2.3	2.9	310	61.7	17.3	0	12.7
SEP 2018	65.1	22.5	2.8	4.5	2.5	2.8	325	60.6	18.7	0	13.5

The isothermal calorimetry test with a curing temperature of 23°C was used to measure the early age heat of hydration of the new Class H cement paste with a w/c ratio of 0.38. Figure 9 shows the heat generation comparison between the two Class H cements. The hydration behaviors of both Class H cements are very similar, which is expected since the two materials have very similar chemical properties. Then, the early age degree of hydration based on the new cement was obtained and compared to the material model calculations shown in Figure 10. The model's prediction seems to have a better agreement with the new cement testing than the previous one. However, there are still some deviations from the model with the test results since the chemical composition used in the calculation was based on the Mill Test Report which may not be the same as the cement sample tested.

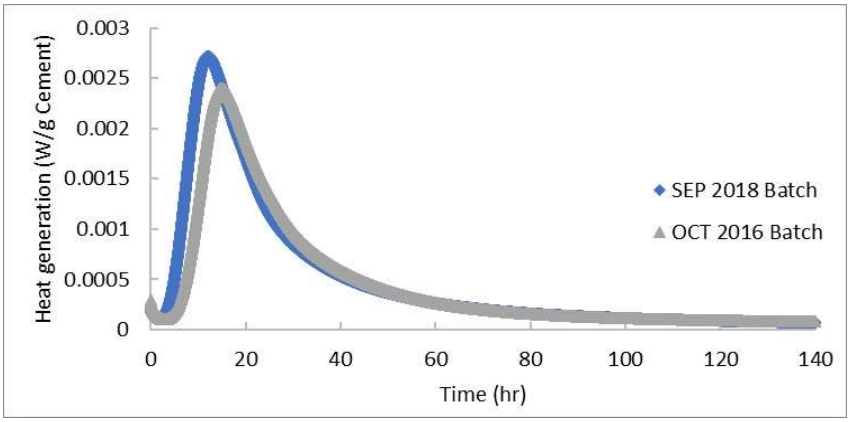

Figure 9: Comparison of heat generation between two Class H cement productions

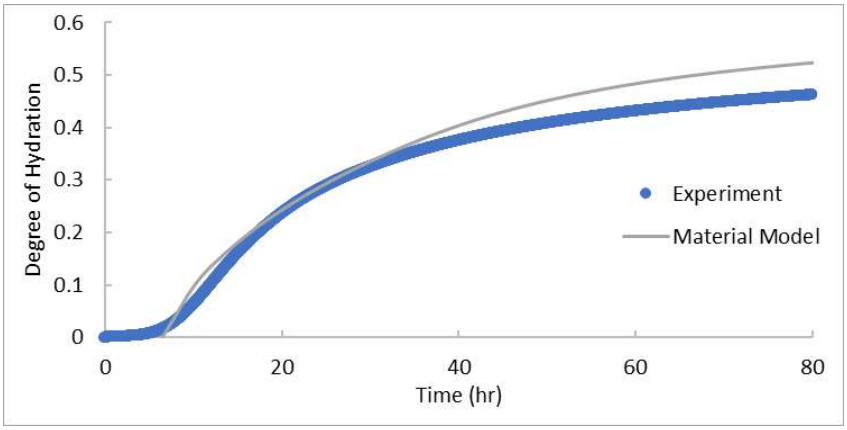

Figure 10: Estimation of degree of hydration of the new Class H cement (September 2018 batch)

Additionally, the isothermal calorimetry was used to measure the heat production of the Class H cement paste with different foam qualities (10%, 20%, 30%) using FAW-20. The water- cement ratios were kept as 0.38 for all the specimens. The isothermal samples were prepared with the following quantity. Each calorimetry bottle has a volume of 24.5854 ml. Therefore, based on the total volume and water-cement ratio, the amount of cement and water for the neat mix (0%) can be calculated to be 35.2499 gram and 13.3949 gram, respectively. Then, for each foam quality, the cement and water amount were reduced based on the increment of the air volume for each quality. 0.0151 ml of FAW-20 foam stabilizer per gram of cement were added. Thus, the admixture amounts were simply obtained by multiplying the mass of cement by 0.0151. The mix proportions of different foam qualities are shown in Table 4.

Table 4: Mix proportions

Foam Quality	Cement (g)	Water (g)	FAW-20 (ml)
0%	35.2499	13.3949	-
10%	31.0730	11.8077	0.469

20%	27.6210	10.4950	0.417
30%	24.1680	9.1838	0.364

Two specimens were prepared for each foam quality. After water and the admixture were added, the bottle was shaken for a few seconds then the cement was added to each bottle. Then, the sample was mixed by shaking the bottle for about a minute until no solid cement particles were visible. The mass of each bottle was recorded after completing the isothermal calorimetry testing, approximately 6-days. At that point, the cement paste has already hardened. The average measured mass, as well as calculated mass densities and the actual amount of air, are shown in Table 5. The mass densities were obtained assuming the total volume of each bottle is 24.5854 ml. The actual air percentages were calculated based on the assumption that the neat cement paste has a mass density of 1.9786 g/ml. The heat generation and accumulated heat comparison between the three different foam qualities are shown in Figure 11 and Figure 12.

Table 5: Measured mass densities

Isothermal Specimen	Measured Mass (g)	Mass Densities (g/ml)	Actual Air (%)
10%	43.2070	1.7574	11.18
20%	38.4126	1.56241	21.03
30%	33.5166	1.3632	31.10

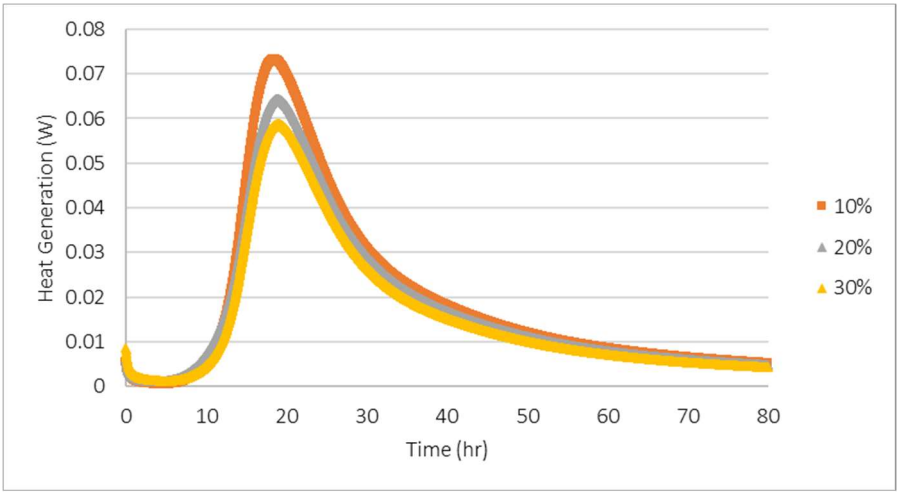

Figure 11: Isothermal heat generation for foamed cement with different foam qualities

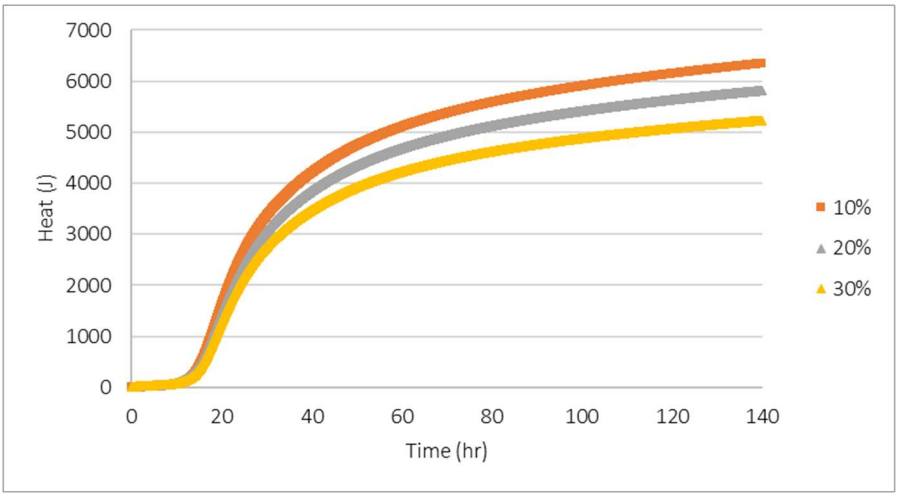

Figure 12: Accumulated heat release for foamed cement with different foam qualities

The heat generation and accumulated heat per unit gram of cement for the foam cement paste with different foam quality (10%, 20%, 30%) and the neat cement paste (0%) are shown in Figure 13 and Figure 14. The normalized heat generation per unit cement mass shows that the amount of entrained air is not an effective parameter for the heat production and the corresponding degree of hydrations. However, as shown in Figure 13, the FAW-20 foaming agent delayed the hydration process. In general, the chemical admixture creates a shell around the cement particles, the coating will delay the cement particles hydration. Also, Figure 14 indicates that in addition to the delaying effect, the magnitude of accumulated heat was reduced during the first 140 hours.

Additional experiments with a higher amount of FAW-20 per unit mass of cement can be helpful to understand the delaying effect of the admixture. To confirm the effect of the admixture and foam qualities on the ultimate heat release, additional isothermal testing with higher curing temperature will be conducted to accelerate the chemical reactions. Preparation of these testing are currently in progress. In addition, during the next phase, modification of the current material model will be conducted so that the model can be sensitive to the air content (different foam quality). This modified model will be a

useful tool for predicting Young's modulus for foamed cement with different foam qualities and different w/c ratio.

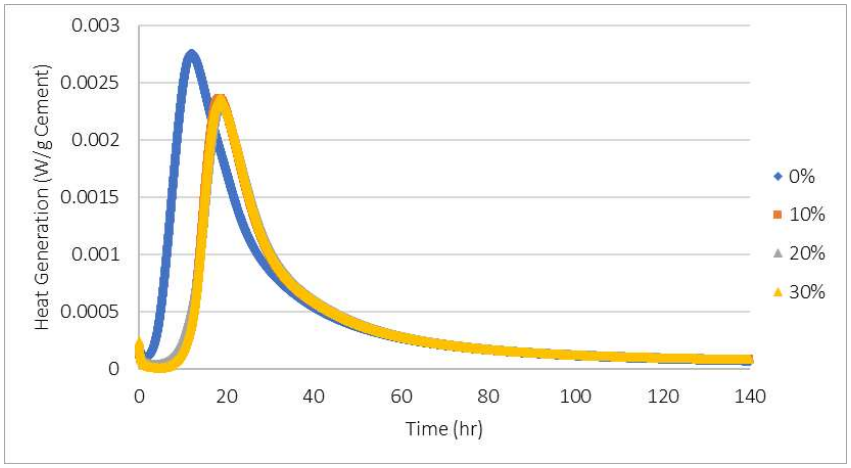

Figure 13: Comparison of heat generation per unit gram of cement for foamed cement with different foam qualities

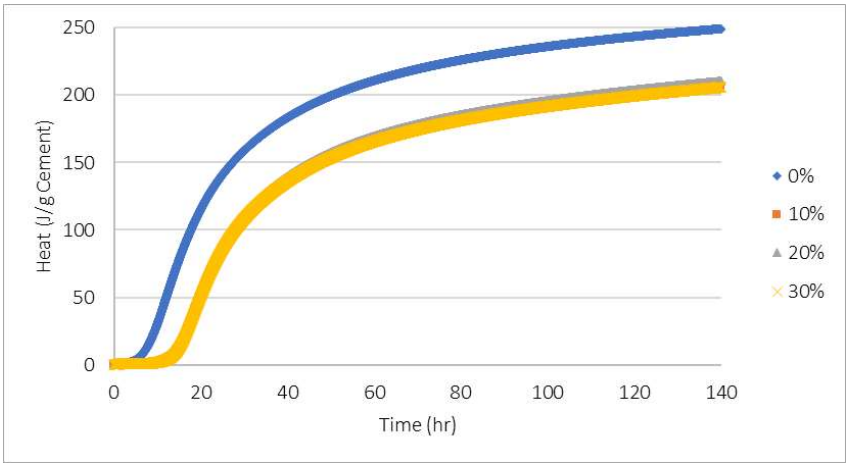

Figure 14: Comparison of accumulated heat per unit gram of cement for foamed cement with different foam qualities